Contents

List of Figures

Introduction

In recent times, some fields of scientific research such as Pharmacology, Molecular Biology, Biochemistry or Neurosciences started to use different new technology concepts in order to obtain a useful data flow from experiments.

These could be, for example, the use of "**smart devices**" that have some particular ability such as identification, interconnection, localization, data processing and external communication. Essentially a "smart device" is an electronic system with several sensors onboard that could interact with the research target and transmit processed or raw data to a "master" device, such as a PC or another "smart device".

Another useful concept is expressed with the term "**Big Data**". This could be described by a set of technologies and methods of analysis of huge amount of data, in order to discover links between different phenomena and predict future ones.

New algorithmic methods are used to predict a specific event. They are represented by new statistical processes to perform identification of patterns within data in order to obtain an adaptive algorithm for that kind of data.

Obtaining this level of quality from scientific research is very important, especially when precise data from each animal subject inside its home-cage are required. Regarding, for example, the study of a particular disease or a pathological condition. Furthermore, in some fields, it is important to achieve also a sort of standardization of data to increase links and exchange of ideas between differents research labs around the world.

It is also important, for a scientific center, that the new introduced device is low cost, given its home-cage compatibility, and the software used is user friendly and open source.

Obviously, all these methods are extremely useful for a researcher, but they should be also more ethical for animals compared to those currently used. When we are talking about high-throughput analysis for animal research used in pharmacological studies or in neurosciences, we are talking about less stressful experiments for the animal, particularly for rodents such as mice and rats.

More ethics in animal research also falls within the fulfillment of the **3Rs**. The principles of the 3Rs (Replacement, Reduction and Refinement)

were developed over 50 years ago providing a framework for performing more humane animal research. This means increasing value and decreasing waste in experimental research.

From this point of view, it is important to maximize the number of data collected directly inside the home-cages in order to have a sort of medical records for each animal used. Each one provided with a registration code.

Rodents are also very susceptible to changes in what they recognize as their habitat and, for this reason, a new environment could introduce states of anxiety or stress. So, usually, to perform an experiment outside their cages they need an habituation period in which the researcher must wait for some time.

Introduction of anxiety or stress could mess up all the useful data, especially in studies regarding drug addiction where stress and anxiety are two meaningful parameters.

Abstract

In the **first chapter** I will introduce the concept of high-throughput analysis methods about animal research and how they can improve extrapolation of scientific information from data through connected 'smart devices'. Then I will discuss about the 3Rs regarding animal welfare and how they will change animal research approaches through new environments and monitoring devices. Until the 'CRACK IT' Challenge established by the NC3R in order to push the market in this direction.

The **second chapter** will describe my work on the development of a liquid level sensor that is able to monitor daily water intake directly inside an home-cage in conformity with the 3Rs tenets, allowing also scientific valuable data from water consumption and animal lickings behavior. This work has culminated in a patent application in collaboration with AM Microsystems.

In the **third chapter** I am going to discuss about my work done for Tecniplast. It concerns data acquisition, data analysis and validation tests on their products and prototypes soon available on the market, not only for research centers but also for breeders that want to add more informations on their phenotypic strains models.

In the **fourth chapter** I will explain how optogenetics works highlighting the main features of this new available technique in neuroscience. I will describe the need for a wireless optogenetics device explaining my work and the results obtained on this purpose.

Chapter 1

High-throughput Analysis for Animal Welfare

High-throughput means all those scientific analysis that can perform tests on a very large number of data in a short amount of time, thanks to automated devices and tools.

This way, you can have software analysis tools (machine learning, neural networks, cloud computing, etc.), hardware *smart* devices able to identify the research subject, acquiring data through specific sensors, transmitting to a remote control system that could be also another *smart* device.

Obtaining a lot of data could be extremely useful for researchers, above all if the data are easy to read and with a high content of information.

1.1 Smart Computing and Sensing Technologies for Animal Welfare

Smart computing and sensing have become common terms to describe next generation computing, communication and sensing technologies and systems, with a broad range of Internet and cloud-based applications and connectivity methods, including combination of various paradigms.

The usage of the term *smart* may vary, but it is typically defined as a networked system connecting physical devices with computing systems for data collection, processing, exchange and analysis, much unlike stand-alone and isolated systems of the past.

Examples of the basic components of smart computing and sensing today are networked devices for wearable computing, wireless and wired sensor and next generation cellular networks, energy efficient computing and sensing systems, and big-data processing and visualization.

These smart technologies are creating, and expected to continue making huge societal and economic benefits in many non-traditional areas. One of

the sectors expected to benefit from the smart computing and technologies is animal welfare in animal research.

The term animal welfare is used to refer to an animal's quality of life. It encompasses the following: animals should be healthy, well fed, and housed in an environment that they might themselves choose; animals should be relatively free from negative states, such as pain, fear and distress, and capable of enjoying life; and animals should be able to carry out behaviors and activities that they are strongly motivated to do.

These concepts could improve also scientific information extrapolated from final data, due to the reduction of anxiety and distress on the animals used for a particular experiment. So, it will be extremely important to monitor all the activities of animals inside their home-cages in order to have an idea of their health conditions before starting a new study.

This can be translated into a new kind of facility, in which electronic devices control many aspects of the animal's life related, for example, to their identification, weighing, food and water intake, vocalization, locomotor activity or social play. Not only from the hardware point of view but also from the software one with new algorithm.

The goal of computational statistics and appropriate algorithm is then to transform raw data in knowledge, finding links, correlations and patterns. All these informations can thus be used by researchers to define an experiment in a better way.

This means that researchers have further informations about their animals besides that obtained from the experiment itself, so the study results in a complete way.

Furthermore, with these methods it is possible to reduce the number of animals used which directly translates into less expensive studies and more ethical animal research.

1.1.1 Smart devices

A smart device is an electronic gadget that is able to connect, share and interact with its user and other smart devices. Some of the most commonly used smart devices are smartphones, tablets, phablets, smartwatches, smart glasses and other personal electronics.

While many smart devices are small, portable personal electronics, they are in fact defined by their ability to connect to a network to share and interact remotely. The different wireless protocols mostly used are Bluetooth, NFC, IR protocols, Wi-Fi, 3G. These allow to operate autonomously, for example by a trigger signal from another device, or directly controlled by users.

An environment in which smart devices can operate is called 'smart environment'. The physical environment is smart because it is embedded or scattered with smart devices that can sense and control part of it.

Cook and Das [10] define a smart environment as "a small world where different kinds of smart device are continuously working to make inhabitants lives more comfortable." Smart environments aim to satisfy the experience of individuals from every space, by replacing the hazardous work, physical labor, and repetitive tasks with automated agents.

In order to have a good readout on what is happening, the environment must be predictive and with decision-making capabilities.

This means that the physical environment may be embedded with a variety of smart devices of different types including tags, sensors and controllers and have different form factors ranging from nano- to micro- to macro- sized.

In addition to the physical environment, it is possible to differentiate also a virtual computing environment.

This virtual environment enables smart devices to access pertinent services anywhere and anytime.

Currently, smart devices are closely related to domotic, fitness or health care. But, in the very next future, as said before, they will be also used in scientific labs because of their features of connectivity, data collection and control of the environment taken into consideration.

In pharmacology, neuroscience or behavioral sciences, specifically, this will lead to a new approach in the management of animal facilities and experimentation.

1.2 3Rs

Continuing improvements to the welfare of animals used in science have occurred over the past few decades partly because of the explicit adoption of a set of principles to guide the ethical evaluation of animal use.

This is the Three Rs tenet: **Replacement, Reduction and Refinement**.

1.2.1 The 3Rs tenet

The tenet is grounded in the premise that animals should be used only if a researcher′s best efforts to find a nonanimal alternative have failed, and that when animals are needed, only the most humane methods should be used on the smallest number of animals required to obtain valid information.

Specifically, **Replacement alternatives** refers to methods that avoid or replace the use of animals in an area where animals would otherwise have been used, including both absolute replacements (replacing animals with inanimate systems, such as computer programs) and relative replacements (replacing more sentient animals, such as vertebrates, with animals that current scientific evidence indicates have a significantly lower potential for pain perception, such as some invertebrates).

Reduction alternatives refers to any strategy that will result in fewer animals being used to obtain sufficient data to answer the research question, or in maximizing the information obtained per animal and thus potentially limiting or avoiding the subsequent use of additional animals, without compromising animal welfare.

Refinement alternatives refers to the modification of husbandry or experimental procedures to minimize pain and distress, and to enhance the welfare of an animal used in science from the time it is born until its death.

The Three Rs tenet also provides a way to focus on the welfare of individual animals rather than solely considering welfare indicators at the level of groups or populations.

Importance of the individual is acknowledged through the requirement to use as few individual animals as possible and to justify how numbers were selected. Similarly, to properly implement Refinement the experience of an animal during proposed procedures and in the housing environment must be carefully examined to identify and mitigate potential harms.

The Three Rs also provides a set of principles that are responsive to new information. This flexibility allows the scientific community to reflect on new empirical knowledge, for example from animal welfare science. Similarly, as ethical values evolve, the Three Rs can respond to such evolution. For example, the principle of Refinement has developed from its original scope of minimizing harms to animals only during experimental procedures. It now includes both minimization of negative states (harms) and promotion of positive states, during the entire lifespan of an animal used in science.

This ethical reflection is an important feature of the Three Rs tenet as it allows practices to be revisited and reassessed in order to continuously improve welfare standards.

The Three Rs tenet also provides a way to balance the needs of science and the needs of animals. The Three Rs framework of utilitarian ethics allows for recognition and acceptance of both the expectations of scientists and the cage-level welfare requirements of the animals. The Three Rs tenet has been successful because many aspects of the Three Rs are essential to good science and good animal welfare. For example, the principle of Reduction has long been closely tied to good experimental design and proper use of statistical methods to determine sample sizes that provide the most scientifically meaningful results.

More recently, providing improved housing conditions for rodents (Refinement) has been shown to result in experimental data with greater scientific validity.

Lastly, the Three Rs tenet assists in improving welfare through its role in uniting disparate groups who have an interest in the welfare of animals used in science, including scientists, veterinary professionals, humane organizations, policy makers and the general public. Within these groups there are varied points of view concerning the acceptability of scientific use of an-

imals; however, the Three Rs tenet provides an approach that is supported by a broad cross-section of opinion, and thus is a uniting ethical concept.

On a practical level, the Three Rs also provides a common language with which to discuss the use of animals in science. This is important both within the scientific community (for scientists, veterinary, and animal care professionals) with its varied research, teaching and testing animal uses, and also between the scientific community, policy makers, the general public, and humane organizations.

The accessibility of the Three Rs tenet is demonstrated by its widespread use in publications from humane organizations, the policies of scientific funding groups, and in regulations and law.

1.2.2 Limitations of 3Rs

Although the Three Rs tenet has achieved some success in improving animal welfare, it has also been criticized for its limitations.

- The Three Rs tenet has been criticized for the underlying premise that the use of animals for scientific purposes is acceptable: providing the criteria for animal use but not allowing for examination of the assumption that use is acceptable [1].

- The Three Rs tenet does not provide a way to give special consideration for certain species. Therefore species with the least public support for their use in science (nonhuman primates and western companion animal species) cannot be exempt from scientific use by solely applying the Three Rs tenet in the ethical evaluation process [3]. In these cases, local institutional policy or legislation are often used to prohibit or limit use of these species, thus bypassing consideration under a Three Rs process. One example is the ban on the use of chimpanzees in science in the United Kingdom, New Zealand, the Netherlands, and Sweden[4].

- Conflicts between each R have also been identified as a limitation, such as the conflict between the goal of reducing overall numbers and the goal of minimizing pain and distress for individual animals (Refinement)[5]. The advent of newer and less invasive methods of data collection such as telemetry and imaging technologies makes it possible to re-use animals; however, this reduction strategy has the potential to increase harm to individual animals, and so must be carefully balanced.

- There can be conflicts between the Three Rs tenet and the goals of certain types of scientific animal use. For example, in some research, such as studies of wildlife populations, Replacement may not be a valid

goal [6]. In addition, in some research and testing the creation of a poor welfare state is the aim of the use (as opposed to a consequence of the use). This is clearly in conflict with Refinement and goal of improving welfare.

- The full potential of the Three Rs tenet to improve animal welfare has not yet been reached and has been identified as an area for renewed focus for the scientific community. Some suggestions to overcome this limitation include increasing efforts to share knowledge through more complete publication of Three Rs-related information in published scientific papers [1, 2] and increasing funding for the development of viable Replacement alternatives

1.3 Standardization of Animal Research Data

One of the oldest principles in biomedical and pharmacological research is to guarantee comparability and reproducibility of results within and between laboratories.

This is especially true in tests for regulatory purposes.

1.3.1 Additional Variables in Experimentation

The use of historical control data is common practice in comparing and interpreting research results, but variations in results, due for example to experimental conditions or different environment, can make it unreliable. Among others, experimental conditions are believed to affect experimental results [7].

Housing conditions are believed to have an important environmental influence on rodent research results. In general, standardization of housing conditions has led to stimulatory poor conditions, as cages only contain features such as food, water, bedding and litter material.

There are also other variables that may need to be considered, particularly those related to behavior, stress, and growth conditions. These variables include acclimation to a new environment (when animals are shipped by the vendor or moved from the animal facility to a procedure room), other environmental effects (temperature, humidity, noise, lights), littermate size, and pheromone effects.

These additional variables can be very important depending on the biologic readout. Moreover, environmental effects, such as avoidance of large temperature changes unless approved as part of an animal protocol, are expected to be part of the normal procedures of humane treatment of animals.

All these variables can be easily monitored using *smart* devices inside the home-cages with collected data transmitted to a recording and storage center, accessible by the users.

Another important parameter to take into account are routine procedures, such as personnel entering the animal room, food and water supply, cage movement and cleaning, body weight determination as well as visual and physical examination. These procedures may cause significant stress to animals [8].

For instance, entering the animal room triggers endocrine and cardiovascular responses, but, in general, this could be significantly reduced by using soundproofed cages and an automated light system.

Also a repetitive procedure as cage cleaning is mostly seen as a rather simple procedure and thought to have minor effects on animals.

Yet, cage cleaning is a disturbing breeding routine accompanied by noise and loss of territory and can be associated with a significant increase in activity, blood pressure and heart rate in rats.

Anyway, animal research instruments sellers are moving along this way, following this trend. Water supply problem is currently solved by, for example, the Automatic Watering Systems®(AWS) integrated on the Tecniplast DVC™new racks.

But the functionality and the results of these new methods and devices must be tested and proved, giving rise to other types of problems.

From my point of view, during my Ph.D., I had to deal with this kind of issues. Working in collaboration with companies to reach a valid result in order to obtain a valid instrument capable of solving these new problems in animal research.

1.3.2 'CRACK IT' Challenges

The NC3Rs is the National Centre for the Replacement Refinement & Reduction of Animal Research in the UK. Their aim is to advance the 3Rs by focusing on their scientific impacts and benefits. NC3Rs also re-defined the standard 3Rs definitions so that they are more reflective of contemporary scientific practice and developments.

NCRs new definition of the 3Rs is:

- **Replacement**: Accelerating the development and use of models and tools, based on the latest science and technologies, to address important scientific questions without the use of animals.

- **Reduction**: Appropriately designed and analysed animal experiments that are robust and reproducible, and truly add to the knowledge base. Sharing data and resources (tissues, brain slices, animals) between research groups and organisations can also contribute to reduction.

- **Refinement**: Advancing research into animal welfare by exploiting the latest *in vivo* technologies and by improving understanding of the impact of welfare on scientific outcomes.

The NC3Rs, science-led and evidence-based, fund research and early career researchers or scientists, foster collaborations between universities and industry to develop and commercialise 3Rs technologies, and provide information on the latest advances to put the 3Rs into practice. One of these projects is the **'CRACK IT' Challenges**.

'CRACK IT' is the NC3Rs response to the changing environment in the biosciences. The aim is to accelerate the availability of technologies which will deliver:

- measurable 3Rs impacts,
- new marketable products,
- more efficient business processes.

The pharmaceutical, chemical and consumer products industries are increasingly outsourcing research, collaborating pre-competitively to reduce attrition and open to novel approaches to reduce animal use. Greater knowledge of the limitations of the animal models, for example, the lack of translation of some findings in animals to humans has led to an urgent need for more predictive, human-relevant systems for efficacy and safety research. Often, industry seeks solutions to this challenge from the academic and small-medium enterprise sectors.

For example, one of the challenges for 2018, sponsored by *MRC Harwell Institute*, is focused on the realization of a food intake measurement device, called **MOSHERS** that stand for **MOuse Smart HoppERS**.

This proposal comes mostly from some important problems found in research activities. One problem is that monitoring food intake needs specialist equipment and space, this requires to disturb animals every day, or, another problem is that the animals behaviour changes when mice are singly housed (Fig.1.2).

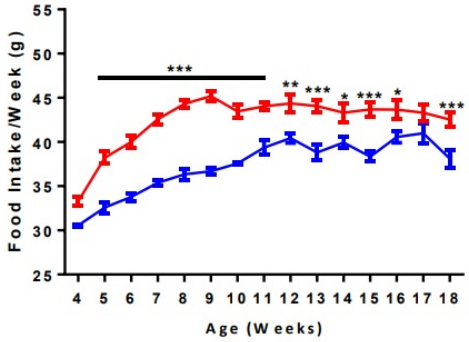

Figure 1.1: [Lee Moir et al.] Home cage food intake monitoring in male $Otp^{R108W/+}$ mutation mice (red) and control group (blue). This mutation expresses a propensity to obesity and a higher consumption of food. [11]

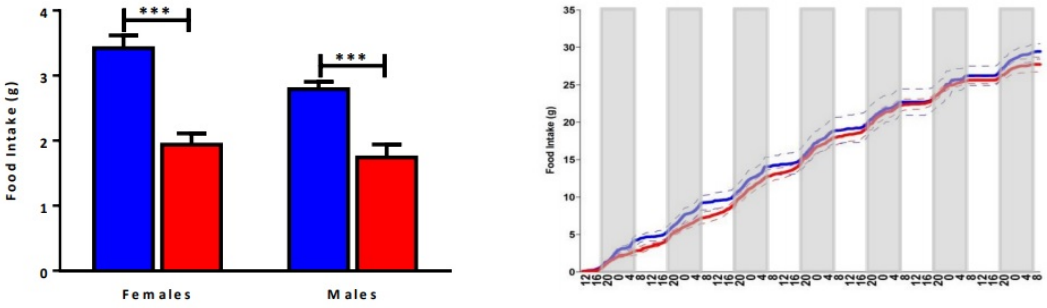

Figure 1.2: [Lee Moir et al.] Food intake using two separate metabolic cage-type monitoring systems. Behaviour changes significantly when mice are singly housed (mutant group in red, control group in blue).[11]

From the results of this paper [11] it is possible to assume that confounding factors such as neophobia and anxiety may be affecting the animal's feeding behaviour.

So, the overall aim of this challenge is to develop a device to accurately measure individual food intake, in real time, in group-housed mice (3 to 5 mice per cage) to avoid these kinds of problems.

The device should be affordable, compatible with all types of mouse caging and data should be easy to collect, analyse and interpret.

The 3Rs benefits from the development such device are:

- A non-invasive way of measuring food intake with no cost to the animal in terms of stress of physical confinement in novel surrounding.
- Information that will be vital in refining the care and analgesia as animals recover from procedures such as surgery.
- Food intake can be used as a proxy for well-being and as an earlier humane endpoint to weight loss (food intake is affected before an effect on weight is seen), allowing many types of studies and mouse models to be refined.
- Database of mouse feeding patterns could be utilised when designing experiments involving food restriction, weight monitoring, energy balance and/or metabolic mutants. This would allow refinements in experiments such as being able to restrict fasting periods to the minimum effective time needed for the physiological response required, avoiding prolonged periods of starvation.
- For diabetes, obesity and metabolism studies, the ability to take accurate and repeated measurements would improve the statistical power

of the experiments, reducing the numbers of animals used. The added value of being able to track diurnal cycles in animals without any concomitant increase in welfare costs to the individual animal would also deliver significant scientific benefits.

- Compatibility with all cage types provides an opportunity to refine and reduce across a wide range of studies (welfare monitoring, recovery from surgery, metabolic studies, phenotyping, drug development, toxicology etc.).

Following these resolutions presented by the NC3Rs, I started a collaboration with AM Microsystems s.r.l. for developing a food intake measurement device in order to partecipate to this challenge, starting from the knowledge acquired by the development of the Chora^{TM}feeder [9] (Fig.1.3) born from a cooperation between the Italian Institute of Technology and AM Microsystems.

1.3.3 Chora^{TM}Feeder

The Chora^{TM}feeder is a device developed to perform home cage work-for-food behavior in mice. It consists of a programmable food dispenser with different cues, such as colour lights and speakers. It collects data and sends them to a Big Data Recorder through a software called Phenopy, developed by the Italian Institute of Technology.

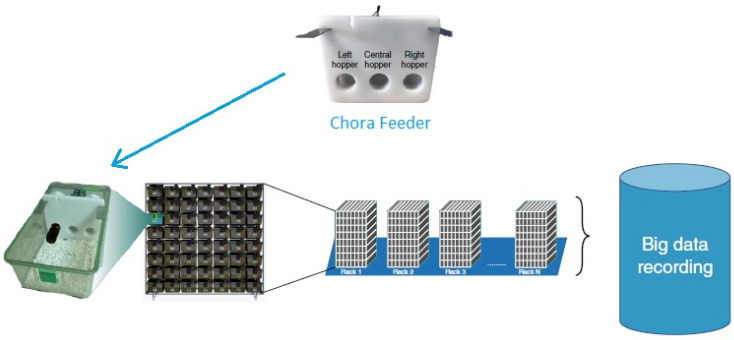

Figure 1.3: Home cage work-for-food system implemented using the Chora^{TM}feeder [9]

Obtaining data from a feeder is important, but it is useless if you can not trace back to the rodent that is eating. The only way to get this information is to equip the animals with a subcutaneous micro-device as a means of identification (RFID tag). This allows also a better standardization in data acquisition for the management of a big facility.

Usually the subcutaneous micro-device is a small electronic tag capable of storing data like a simple code number. This code number represents the animal during a test. Then, another external electronic device activates the tag through a tuned antenna at a proper radio-frequency allowing the readout of the code number.

This technique is called **Radio-Frequency IDentification (RFID)**.

The low frequency electromagnetic waves emitted by an RFID device are totally harmless for the animals (LF-RFID standards are 125 kHz and 134.2 kHz).

On the Chora^{TM}Feeder the hoppers radius are 1.5 cm, the RFID antenna must be fixed around them with a radius of 2 cm. So, starting from the Faraday's law of induction (1.1), we can calculate the electromotive force, Σ, induced on the coil of the tag antenna.

$$\Sigma = -N_2 \frac{d\Phi}{dt} = -N_2 \frac{d}{dt} \int \vec{B} \cdot d\vec{S} = -M \frac{d\vec{I}}{dt} \tag{1.1}$$

In which N_2 are the turns of the coil tag antenna, $\vec{B}$ is the magnetic field generated by the reader, M is the mutual inductance (1.2) and $\frac{d\vec{I}}{dt}$ is the variation over time of the current on the reader antenna.

$$M = N_2 \left[\frac{\mu_0 N_1 a^2}{2(x^2 + r^2)^{\frac{3}{2}}} (b^2 \pi) \right] \tag{1.2}$$

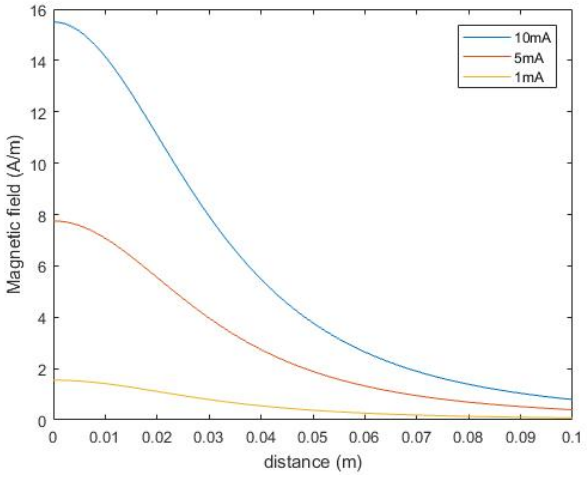

Figure 1.4: Magnetic field strength of a circular loop antenna (d=4 cm, w=2 mm, h=1.5 mm, 124 turns) for different values of current, as a function of the distance.

Knowing the diameter (b) and the turns of the coil on tag antenna, from the mutual inductance (1.2) it is possible to calculate the magnetic field intensity as a function of the current on the reader antenna at different distance (x) (Fig.1.4).

An antenna of this type can detect the RFID tag, for a frequency of 134.2 kHz, at about 3 cm with a reasonable energy consumption for a battery powered system.

This allows to monitor directly inside the home-cage the work-for-food test for each different animal into the cage.

Moving further, it is extremely useful to monitor also water intake. From this idea I developed a liquid level sensor in collaboration with AM Microsystems S.r.l.

Chapter 2

Liquid Level Sensor

2.1 Introduction

Daily water consumption is an important data for a commercial animal breeding facility, for example, that monitors and controls all their different animal specimens regarding both their health status or sales information. Alternatively, daily water consumption data are useful for a research lab facility, in which monitored water intake could be meaningful in many researches regarding different systems such as physiologic, metabolic, neurologic, endocrine, behavioral, etc.

Currently water intake is measured by weighing the filled water container, embedded in a new specific cage, at the starting point of the experiment and at any other time point, respecting a particular protocol.

This approach is not very appropriated for the animals. It could introduce stress and anxiety states, especially in those individuals most prone to neophobia, as discussed in the first chapter about the new environment of a new cage. Moreover the researcher could disturb the normal activity of the animal just enetring the room.

For these reasons it is important to achieve useful informations about water intake, or any other relevant information, directly inside a cage using wireless technology and smart electronic devices.

In order to reach these specifications I choose capacitive sensing technology.

2.2 Capacitive Sensing

Capacitive sensing is becoming a popular alternative to other methods in applications of proximity detection, material analysis and liquid level sensing.

The main advantages that capacitive sensing has over other detection approaches are the capability to sense different kinds of materials (organic

tissue, metal, liquid etc.) together with specifications of being contactless and wear-free with a large sensing range, small form factor of low cost PCB sensors and low-power consumption.

Capacitive sensing is based on the measurement of capacitance variation. Capacitance (C) is the capability of a body to store electrical charge (Q) at a given voltage (V) and it is calculated as:

$$C = \frac{Q}{V} \tag{2.1}$$

2.2.1 Conventional Configuration

The conventional configuration of a capacitor is composed by two parallel plates of a conductor material on which an electrical potential is applied. Plates are separated by a dielectric material that could be any electrical insulator that can be polarized by an applied electric field.

Because of dielectric polarization, positive charges are displaced towards the field and negative charges shift in the opposite direction. This creates an internal electric field that reduces the overall field within the dielectric itself.

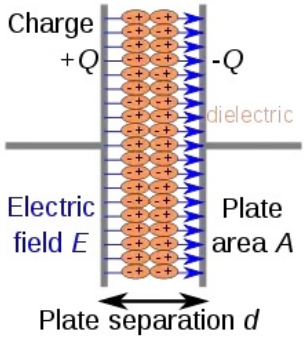

Figure 2.1: Dielectric polarization in a conventional configuration of a capacitor.

From Gauss's law we obtain the magnitude of the electric field between the plates defined as $E = \frac{\sigma}{\varepsilon}$, in which $\sigma = \frac{\pm Q}{A}$ is the charge density and ε is the electrical permittivity.

The voltage between the plates is defined as the line integral of the electric field over a line from one plate to another (2.2).

$$V = \int_0^d E(x)dx = \frac{\sigma}{\varepsilon}d = \frac{Qd}{\varepsilon A} \tag{2.2}$$

So, getting equation 2.1 and replacing V we obtain the capacitance as a function of geometrical dimension and electrical permittivity only.

$$C = \frac{\varepsilon A}{d} \tag{2.3}$$

The difference of permittivity between vacuum ($\varepsilon_0 = 1$) and air ($\varepsilon_{air} = 1.0006$) can often be considered negligible, but this is not true for all those dielectric materials, such as water for example ($\varepsilon_{water} \simeq 80$), with a high relative permittivity.

So, in general, for any material different from air, the dielectric permittivity is written as the product between the vacuum permittivity and the relative permittivity of the material ($\varepsilon = \varepsilon_0 \varepsilon_r$). From equation 4.15 we obtain then:

$$C = \frac{\varepsilon_0 \varepsilon_r A}{d} \tag{2.4}$$

In case of variation of the physical quantity of dielectric material inside the capacitor, we have to consider the variation of the area filled by the new dielectric material with respect to the area occupied by air, multiplied by the relative electrical permittivity.

2.2.2 Coplanar Configuration

We saw that the capacitance of capacitive electrodes depends on the geometrical shape of the conductor-dielectric arrangement and position in the electric field.

So, it is reasonable to expect that a different configuration gives us a totally different response and this will be proved.

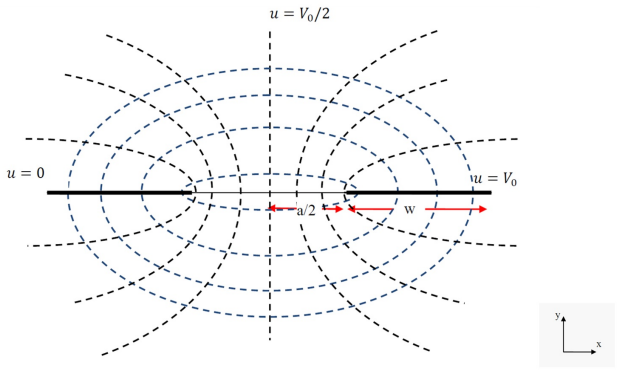

Figure 2.2: Electric field configuration of a two dimensional coplanar electrodes. In black the equipotential lines and in blue the electrical flux lines.

As we can see from Fig.2.2 a coplanar configuration of electrodes, at which a potential difference is applied, creates an electric field that exists not just directly between the conductive plates, but it extends some distance away, and this is known as **fringing field**.

Using this configuration allows us to apply any kind of material between the two electrodes.

The fringing electric field of the coplanar plates penetrate into the material, thus any variation of the dielectric property affects the inter electrode capacitance readout.

The solution for the two dimensional electric field distribution in this configuration of electrodes can be found using the inverse discrete cosine transform by which a coordinate $Z = x + iy$ in the rectangular x-y plane is converted to $W = u(x, y) + iv(x, y)$ in the inverse cosine u-v plane, where the equipotential lines $u(x, y)$ are hyperbolic (Fig.2.2) and the electrical flux lines $v(x, y)$ are elliptical [12].

So, from the inverse cosine transform:

$$W = V_0 - \frac{V_0}{\pi} \cos^{-1}\left(\frac{2Z}{a}\right) \tag{2.5}$$

We can write:

$$Z = \frac{a}{2} \cos\left[\frac{\pi}{V_0}(V_0 - W)\right] \rightarrow x + iy = \frac{a}{2} \cos\left[\frac{\pi}{V_0}(V_0 - u) - i\frac{\pi}{V_0}v\right] \tag{2.6}$$

This allows to obtain x and y coordinate values in terms of u and v (2.7 and 2.8)

$$x = \frac{a}{2} \cos\left[\frac{\pi}{V_0}(V_0 - u)\right] \cosh\left(\frac{\pi v}{V_0}\right) \tag{2.7}$$

$$y = \frac{a}{2} \sin\left[\frac{\pi}{V_0}(V_0 - u)\right] \sinh\left(\frac{\pi v}{V_0}\right) \tag{2.8}$$

Hence, the equations of elliptic (2.9) and hyperbolic (2.10) lines (Fig.2.2) are derived as follows

$$\frac{x^2}{\cosh^2\left(\frac{\pi v}{V_0}\right)} + \frac{y^2}{\sinh^2\left(\frac{\pi v}{V_0}\right)} = \frac{a^2}{4} \tag{2.9}$$

$$\frac{x^2}{\cos^2\left[\frac{\pi}{V_0}(V_0 - u)\right]} - \frac{y^2}{\sin^2\left[\frac{\pi}{V_0}(V_0 - u)\right]} = \frac{a^2}{4} \tag{2.10}$$

To solve the total electric charge on the electrodes, when all the electric charges are assumed being located on the electrode surface ($y = 0$) (since

the thickness is negligible in comparison to the electrode width) Gauss's law is applied.

$$Q = \iint D(y=0)dA \tag{2.11}$$

In which the electric displacement vector is defined as

$$D(y=0) = -\varepsilon_r \varepsilon_0 \left(\frac{\delta u}{\delta y}\right)_{y=0} \tag{2.12}$$

$\frac{\delta u}{\delta y}$ can be derived from equation 2.8. The boundary condition of $u = V_0$ at the surface w on the plane $y = 0$ gives:

$$\left(\frac{\delta u}{\delta y}\right)_{y=0} = -\frac{2V_0}{a\pi \sinh\left(\frac{\pi v}{V_0}\right)_{y=0}} \tag{2.13}$$

So, from equation 2.12 we have:

$$D(y=0) = \varepsilon_r \varepsilon_0 \frac{2V_0}{a\pi \sinh\left(\frac{\pi v}{V_0}\right)_{y=0}} \tag{2.14}$$

And solving 2.11 for Q we obtain

$$Q = \frac{2\varepsilon_r \varepsilon_0 l V_0}{\pi} ln \left[\left(1 + \frac{2w}{a}\right) + \sqrt{\left(1 + \frac{2w}{a}\right)^2 - 1}\right] \tag{2.15}$$

Hence, the capacitance, expressed by $C = \frac{Q}{V_0}$, of two dimensional coplanar electrodes is:

$$C = \frac{2\varepsilon_r \varepsilon_0 l}{\pi} ln \left[\left(1 + \frac{2w}{a}\right) + \sqrt{\left(1 + \frac{2w}{a}\right)^2 - 1}\right] \tag{2.16}$$

The width of the sensing electrodes (w) establishes the maximum field penetration depth, T, along the $\hat{y}$ direction. It can be deduced from the elliptical contours $v(x, y)$ and corresponds to the maximum $\hat{y}$ displacement of field line. This also give us a measure of sensitivity of the coplanar electrode pair, that is calculated as

$$T = \frac{a}{2}\sqrt{\left(1 + \frac{2w}{a}\right)^2 - 1} \tag{2.17}$$

From equation 2.16, it is possible to rewrite the capacitance in terms of penetration depth T.

$$C = \frac{2\varepsilon_r \varepsilon_0 l}{\pi} ln \left[\frac{2}{a}(T + \sqrt{T^2 + 1})\right] \tag{2.18}$$

Finally, we can calculate the capacitor sensitivity along $\hat{z}$ axis from the changing difference between electrical permittivity of air and liquid inside the container.

$$\Delta C = \frac{2(\varepsilon_r - 1)\varepsilon_0 \Delta l}{\pi} ln \left[\frac{2}{a}(T + \sqrt{T^2 + 1}) \right] \tag{2.19}$$

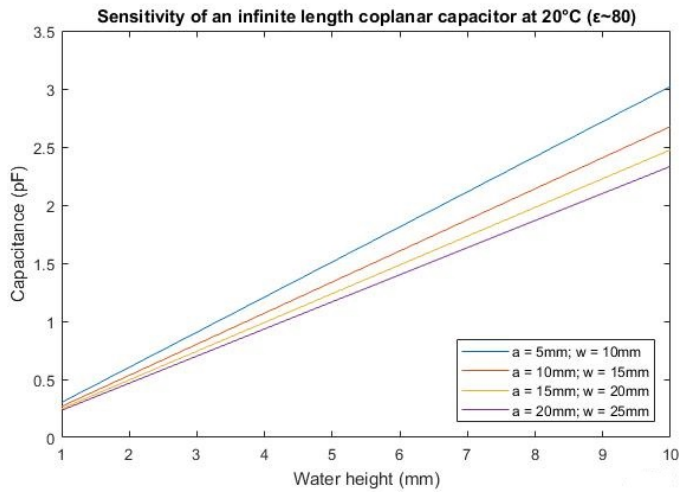

Figure 2.3: Capacitance variation due to 1 mm height change of dielectric permittivity from air to water along $\hat{z}$ axis.

From the graph trends 2.3 and equation 4.9 it is clear that to maximize sensitivity of the device it is necessary to increase the field penetration depth, by increasing width of electrode (w) or minimizing the gap separation (a).

Considering the dimensions of the standard bottles used in our Lab facility and the dimensions of the Printed Circuit Board (PCB) I chose, for my purpose, a gap separation between electrodes of 5 mm and a width of 10 mm.

Multi-dielectric layers

The capacitive sensing using the coplanar plates topology allows a high sensitivity to dielectric variation along the $\hat{z}$ axis, this makes it a useful technique to measure liquid inside a container without interfere with it. But, the container could introduce a parasitic capacitance to the measurement along the $\hat{y}$ axis.

Fig.2.4 shows the model of a liquid level sensing coplanar plate capacitor which comprises multi dielectric layers.

The total capacitance can be represented as a sum of capacitance components.

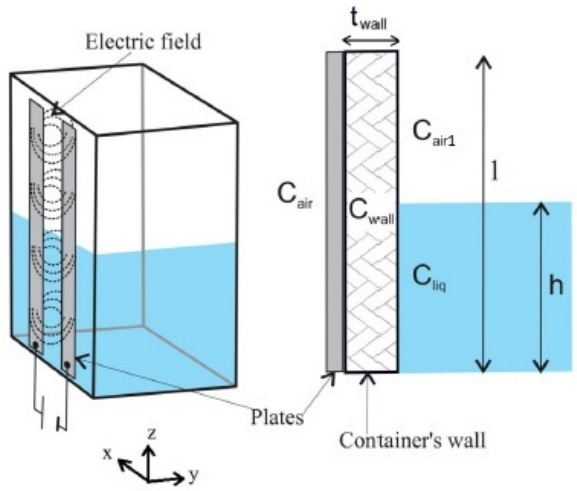

Figure 2.4: Configuration of the coplanar plates capacitor in a liquid level sensor.

$$C_{tot} = C_{air} + C_{wall} + C_{liq} + C_{air1} \tag{2.20}$$

The contribution to the variation of total capacitance C_{tot} is mainly given by the variation of the liquid capacitance with respect to that of the air. Other contributions are costant and too small ($\varepsilon_{plastic} \sim 2.5$) to be considered. So, the variation of the total capacitance could be represented as a sum of a costant capacitance (C_0) and the liquid height contribution.

$$\Delta C_{tot} = C_0 + h(\varepsilon_{liq} - \varepsilon_{air}) f(a, w, l) \tag{2.21}$$

In which $f(a, w, l)$ is a function that depends on electrodes dimensions. The system is then setted at $C_0 = 0$ in order to have a starting point indicating the empty container.

2.2.3 Out Of Phase (OoP) Technique

Conventional Approach

Capacitive sensing is usually implemented in a conventional ratiometric approach. This is done using a capacitive-to-digital converter with one of the two electrodes that compose the coplanar capacitor driven to ground (Fig.2.5).

A key aspect of this approach is that all the sensors are driven with the same excitation signal. Changes in excitation signal due to changing

capacitance are measured and used to calculate the corresponding liquid level. This is possible thanks to the differential measurement allowed by the integrated circuit (FDC1004 in this case).

In this approach **Shielding electrodes** prevent external interference and also block the electric field lines behind level electrode and the grounded one (Fig.2.5) focusing the readout signal only on the container. **Reference electrodes (RL and RE)** are added in order to have the maximum (full container) and minimum (empty container) value of capacitance to calculate the level of the liquid at any interval height.

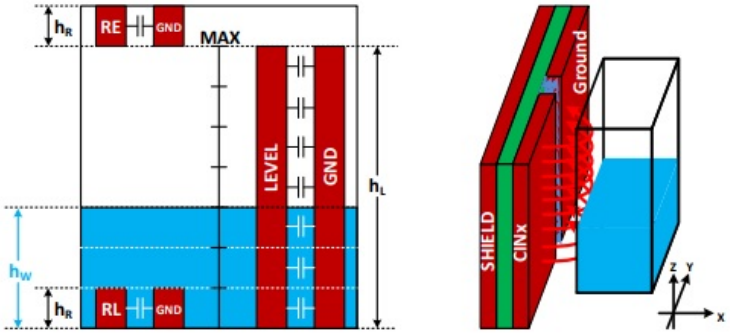

Figure 2.5: Conventional ratiometric approach for capacitive sensing in which electrodes are driven to ground and shielded [13].

$$Level = h_{RL}\frac{C_{level} - C_{level}(0)}{C_{RL} - C_{RE}} \tag{2.22}$$

Where h_{RL} represents the unit height of the reference liquid electrode. A perfect symmetry on the dimensions of different electrodes is mandatory if we want to obtain a precise measurement, in my case $h_{RL} = \frac{1}{10}h_{level}$.

This configuration allows to obtain a liquid and temperature independent measurement system, but it does not prevent from any grounded interference noise or electromagnetic source of noise.

This noise could be very significant if we consider that this device could be in proximity of human body or if someone touches it during a measurement, because our body can be seen as a grounded capacitance (Fig.2.6).

Once the human body presence (human hand) is in close proximity to the liquid source, an additional parasitic capacitance is introduced into the model and causes the potential difference due to the liquid to change relative to the absence of the hand.

An alternative approach to mitigate this additional parasitic capacitance is the Out-of-Phase (OoP) technique.

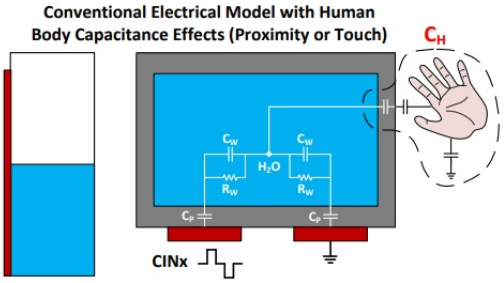

Figure 2.6: Representation of a conventional capacitive sensing approach with a coupled human body capacitance [13].

Out-of-Phase Approach

The Out-of-Phase technique is based on the symmetry of the electrodes configuration and replaces the grounded electrodes with the shielding electrodes (SHLDy) that are driven in 180° out of phase with respect to the sensor electrodes (CINx).

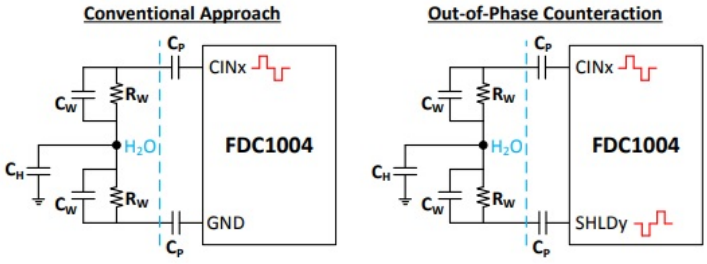

Figure 2.7: Comparison between conventional approach and out of phase electrical model [13].

As we can see from Fig.2.7, the signal from the grounded electrodes in the OoP configuration is now driven in phase opposition from the FDC1004, in this way node C_H is maintained at a costant potential. This allows to obtain a very significative decrease of noises from external sources, like for example human hands contact.

This approach could be possible only with a particular layout of electrodes (Fig.2.8), in which the two external electrodes are driven by the SHLD2 Input Pin, thus replacing the ground electrode on the conventional approach, and the Level electrode (CIN1) and the Reference electrode (CIN2) are driven in phase with the shielding electrodes (SHLD1).

The phase opposition between the sensor electrodes and the SHLD2 electrodes is now established.

Thanks to the differential mode operation of the integrated circuit, it is possible to obtain two capacitance signal readouts from the Reference electrode (RL) and the Level electrode subtracting the channel CIN4 that is set as negative input in phase with SHLD2.

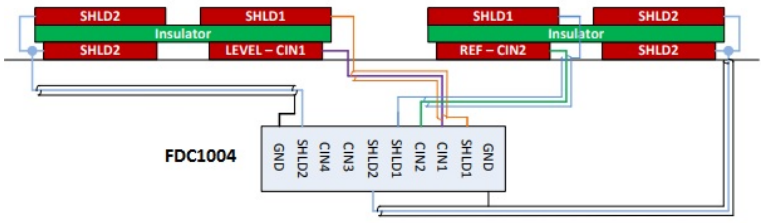

Figure 2.8: Out-of-Phase electrodes configuration and connections with the capacitive-to-digital converter (FDC1004) [13].

Considering the two signals obtained with this method and using Eq.2.22, in which RE value has been replaced with a blank reading signal acquired from the Reference electrode, the liquid level is finally given according to Eq.2.23 in which $Meas1 = CIN1 - CIN4$ and $Meas2 = CIN2 - CIN4$

$$\Delta C = h_{RL} \left[\left(\frac{1}{n} \sum_{i=1}^{n} \frac{Meas1_i}{Meas2_i} \right) - \frac{C_{level0}}{C_{RL0}} \right] \tag{2.23}$$

2.2.4 Calibration

In order to have good matching values between real data and readout signal from the electronic system we need a precise instrument calibration. To do that, the best method is to obtain a calibration curve useful to understand the instrumental response in some respects.

Signals from the capacitive-to-digital converter are expressed in pF and they are sent, using standard I^2C protocol, to a microcontroller in which a custom program is loaded.

The Eq.2.23 is implemented by the program and it returns an indicative value for the liquid level.

This value is then converted into volume using a calibration curve obtained by interpolation method.

Each point of the interpolation function (2.10) were reported by recording the y-intercept value for a linear regression (2.9) of a data set acquired in a time of 8 minutes. This value corresponds to the mean value for this data set. A set of standard samples were made at steps of 50 ml with this method.

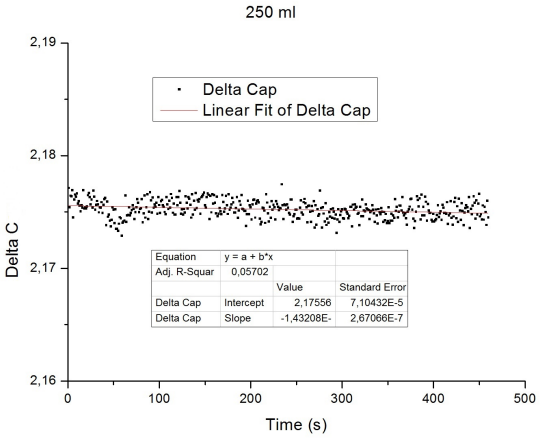

Figure 2.9: Least squares regression line for a set of data at 250 ml.

For better accuracy and to understand the error, the response at each volume was repeated so an error value is obtained. Data are then fitted with a function so that unknown volume's values can be predicted.

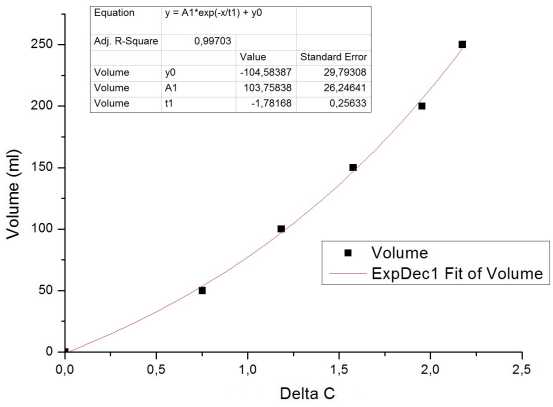

Figure 2.10: Interpolation function used as calibration curve to convert signal readout in unit volume.

This allowed to reconstruct the interpolation function used as calibration curve (Fig.2.10 and Eq.2.24).

$$y = A_1 e^{(-\frac{x}{t_1})} + y_0 \tag{2.24}$$

From the interpolation function, that is an exponential function, it is

possible to deduce that errors on the response are larger at large volume values.

With this method it has been reached an accuracy of $\sim 1ml$ on the signal readout.

2.3 Preliminary Results

Materials and Methods

Currently, the system has been tested in the animal facility of the Unicam's Experimental Medicine Department.

Test was performed in a ventilated room held at the proper temperature of $22°C$ under a normal 12hr-12hr light-dark cycle.

Cage used was the standard GM500 Tecniplast with a dust-free wooden litter and standard food pellets. For rats, a conventional 1500U Tecniplast cage was used. Bottles used for the test were the standard 250 ml both for mice and rats.

Animals used were 2 CD1 male mice and 2 Wistar male rats. Tests were performed for a period of several days depending only on the availability of the animals for this kind of experiment (5 days for mice and 3 days for rats).

Data were acquired using the liquid level sensor connected by USB cable to a PC and a custom dedicated software used only to collect data.

Results

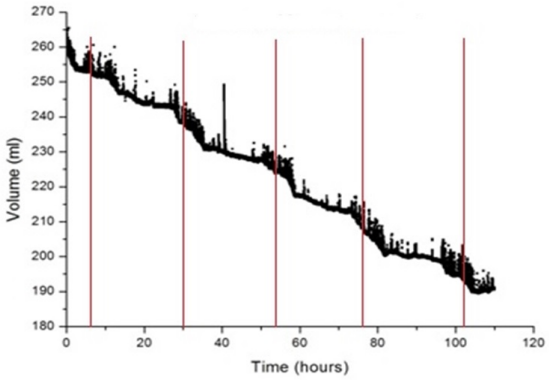

Figure 2.11: Graph shows the decreasing level of water for a cage with 2 CD1 male mice. Red vertical lines are indicating midnight time. Data were acquired during 5 days of continuous acquisition.

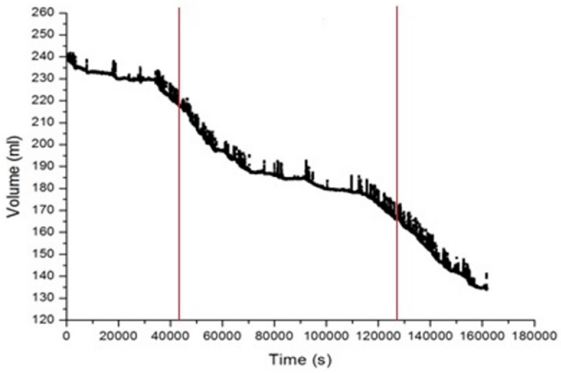

Figure 2.12: Graph shows the decreasing level of water for a cage with 2 Wistar male rats. Red vertical lines are indicating midnight time. Data were acquired during 3 days of continuous acquisition.

The decreasing level of water measured for mice indicates an average daily consumption in water intake of ~ 6.8 *ml* for each individual, assuming an equal amount of water consumed. Relative to rats, the average daily consumption in water intake results ~ 26 *ml* per rat.

Data obtained are in line with general information regarding animal care that reports an average values of daily water intake for mice of 3-5 *ml* and 20-50 *ml* for rats [14]. (*Species Specific Information-John Hopkins University*).

It is interesting also to note the cycle of the circadian rhythm both for mice and rats. Light cycle was normal, so you can clearly see the increasing activity during the night time.

These results on activity monitor, were be possible only using capacitive sensing measurements. Infact, when an animal touches liquid inside the container, it grounds the circuit allowing a coupling capacitance due to its body.

This small parasitic capacitance can be measured by the electronic system creating a little spike in the readout data. These spikes can be used to do analysis of lickings microstructure.

2.3.1 Lickings Microstructure Analysis

Fluid licking behavior in rodents is widely used to determine fluid consumption and greed in various behavioral contexts. This is a highly stereotyped behavior characterized by repetitive tongue and jaw movements.

Typically, this behavior has been measured with 'lickometers' utilizing either electrical, optical or force sensors [15].

Capacitive sensing allows an alternative solution that solves also the problem of measuring liquid intake at the same time.

One mainly problem to achieve this kind of measurements is to be able to electrically isolate the bottle's spout with an insulator. In this case I used thermo-shrinkable wrap only for the time needed in this experiment.

Obviously for a commercial product other materials could be used such as ceramics or high density plastic.

Tests for this kind of analysis were done only in male CD1 mice. To reach a good instrumental sensitivity it is important to acquire data fast enough to be able to follow just a single event. C57BL/6 and DBA/2J mice lick at a frequency of respectively 8.5 Hz and 10.6 Hz [16].

As reported from *J. D. Boughter et al.* there are genetic-based variations in interlick interval (ILI) duration completely independent from sex, extent of water deprivation or total number of licks.

Important parameters are, moreover, the lickings burst size and the pauses duration between different burst [15].

In order to achieve these different parameters I need a sampling rate at least at double the frequency of the analog signal read, as *Nyquist-Shannon sampling theorem* (2.25) says in order to have a sufficient condition for a sample rate that permits a discrete sequence of samples. So a sampling time of $\leq 50\ ms$ is needed.

$$f_{sampling} \geq 2 f_{signal} \tag{2.25}$$

Considering a samples rate of 400 S/s setted on the FDC1004 multiplied by each acquisition channel, I obtain a readout data of $\sim 100\ Hz$ that means a sampling time of 10 ms.

Largely sufficient for the purpose.

So, using these parameters, I perform different acquisition sessions of few minutes in order to have at least one licking behavior, obtaining the following results for different sessions.

From acquired data it is easy to calculate a licking frequency of 9.2 Hz that corresponds to $\sim 108\ ms$ for each event, that is composed both of a lick and a pause. So, a single licking behavior is on average $\sim 54\ ms$ time long, for CD1 mice.

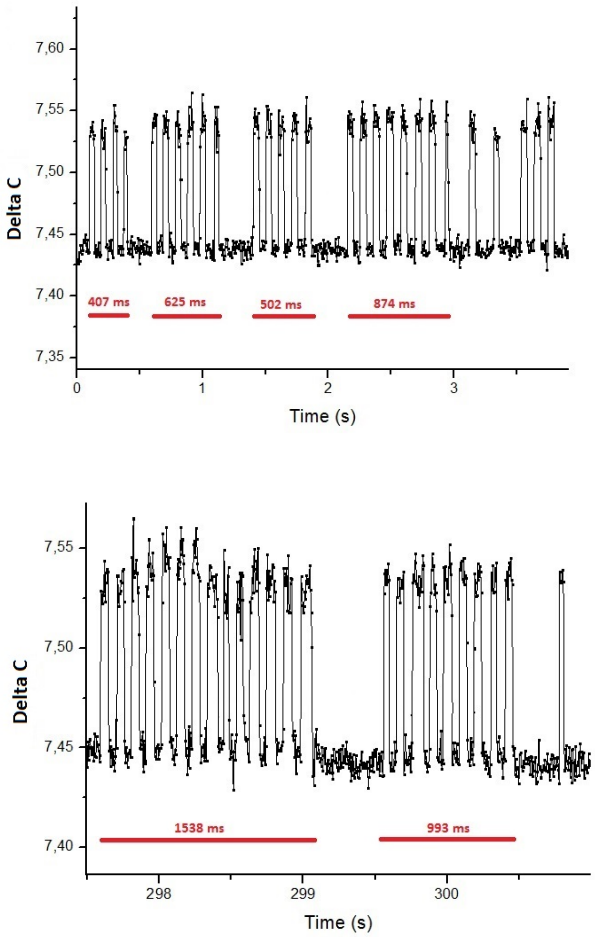

Figure 2.13: Licking Microstructure Analysis performed in CD1 mice. In red each burst duration is highlighted.

2.3.2 Temperature Drift

Basically, the high dielectric costant of water is due to its molecular dipole structure in which the two positive charges of Hydrogen are at the opposite site of the negative charge of Oxygen. This creates a resulting electric dipole moment (Fig.4.12) as $\vec{\mu} = q\vec{d}$ that could be oriented by an external electric field, this is call *Polarization*. The material's ability to store an electric field through polarization effect is the *Permittivity*, represented by relative permittivity ε_r (Eq.2.4) as the ratio between its absolute permittivity ε and vacuum permittivity ε_0.

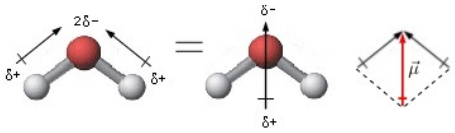

Figure 2.14: Electric dipole moment of water molecule.

In water this effect is increased by Hydrogen bonds between molecules. In fact, Hydrogen atoms are electrostatically attracted by Oxygen atoms of other molecules.

This phenomenon increases a lot the water's permittivity and consequently the water dielectric costant. In this scenario, an increasing temperature introduces an increasing kinetic energy of molecules.

This is capable of destroying weak Hydrogen bonds allowing greater movements of the water's molecules and, consequently, a decreasing of the dielectric costant. So, an increasing temperature introduces a decreasing of water relative permittivity.

Inside a bottle, containing 250 ml of water, a difference of temperature between an initial value (T_i) and room temperature (T_r) is quantified with the calculation of a transient thermal regime.

$$T(t) = T_r + (T_i - T_r)e^{-\frac{hA}{mc}t} \tag{2.26}$$

In which h is the heat transfer coefficient of water, A is the heat exchange surface of the bottle, mc is defined as the heat capacity calculated as the product of the mass and the specific heat of the system.

Assuming an initial value of temperature of 10°C and a room temperature of 25°C degrees, we obtain:

From the Graph 2.15 we can see that, after ∼10 min, we obtain an equilibrium between room temperature and initial water temperature.

The liquid level sensor acquires data using OoP technique in differential configuration and the basic working principle relies on simmetry of the electrodes.

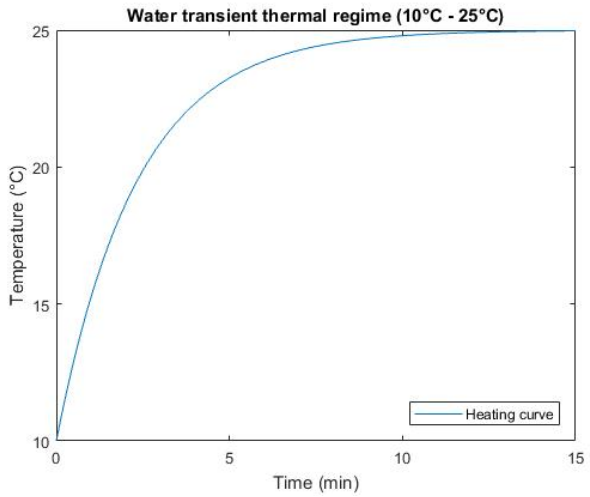

Figure 2.15: Transient thermal regime of the system from a temperature of 10°C degrees to 25°C degrees.

All these expedients should take into account a temperature drift during a measurement, especially on the first minutes of acquisition, because all the readout from the electrodes change simultaneously, following the decreasing dielectric costant due to the increasing temperature.

Obviously, the response in the real world could be slightly different and deviations could occur on final readout data and real measurements.

These deviations are contained by a very precise realization of the printed circuit board.

2.4 Final layout

On the basis of this previous work, I designed a dedicated electronic schematic diagram using KiCad, a free software suitables for electronic design automation.

Electronic schematic diagram is composed of:

- Voltage regulator circuit;
- JTAG connector for programming and debug;
- Bluetooth module ARTIK020;
- Wireless charging antenna and tuning control circuit;
- Capacitive sensing module FDC1004;
- Wireless power rx module BQ51003;
- Battery charger control circuit based on BQ24230;

The schematic was then converted in a PCB layout design (Fig.2.16).

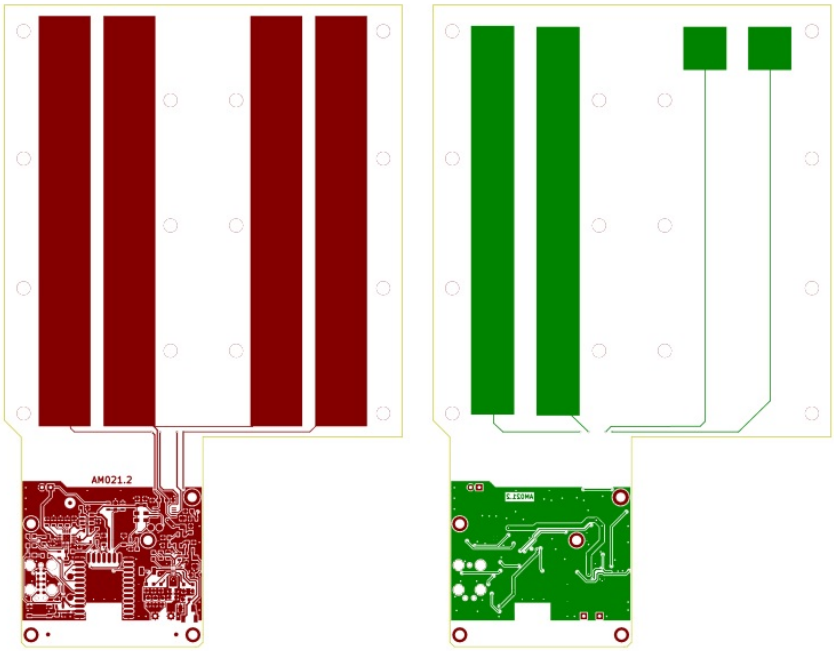

Figure 2.16: KiCad Printed circuit board layout design. In red the back copper layer and pads are indicated; in green the front copper layer and pads.

Battery used is a 3 x 5 cm Lithium Polymer battery 3.7 V, 850 mAh. Sufficient to provide ∼230 hours of continuous operational work in the condition requested by experiments.

Then a case container model has been designed using Onshape (Fig.2.17), an in cloud 3D CAD, and 3D-printed in PLA plastic.

Currently the liquid level sensor is in patenting stage *(Patent application N: 102018000006637)* and further tests are planned in order to provide also a mobile phone application to the customers.

This allows easily accessible data and, therefore, to facilitate data collection for final users.

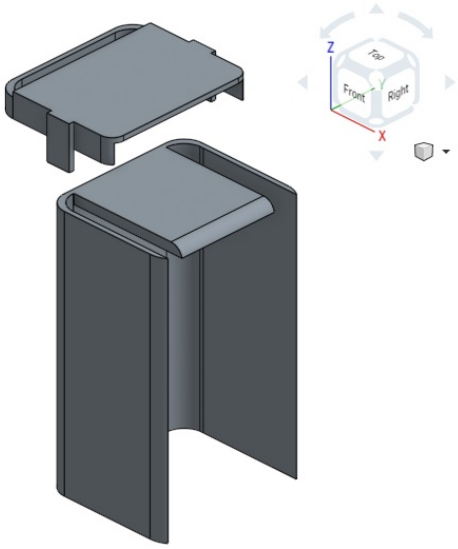

Figure 2.17: 3D model of the bottle container. The 3D printed prototype used in the tests has been designed from this drawing.

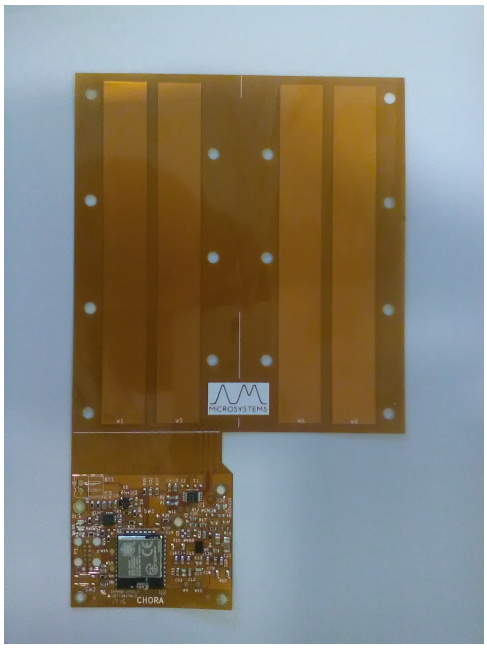

Figure 2.18: Liquid level sensor PCB made in kapton with mounted components.

Chapter 3

Tests on Tecniplast Products

As an Eureka Ph.D. candidate, I also collaborated with Tecniplast S.p.a., a big company of Varese, in the north of Italy, as a customer of AM Microsystems S.r.l. Their core business is to provide new solutions for animal facility such as new cages design, racks and analysis tools for scientific research.

On these perspectives they targeted on creating digital housing solutions within their Digilab project.

My work was focused mostly on data analysis and data acquisition for the validation of their DVC® - Digital Ventilated Cage system (DVC Analytics® for the Big Plate system and DVC Lite®).

3.1 DVC® Lite

3.1.1 Introduction

On their Digilab project, Tecniplast wants to integrates, with their already existing AMS - Animal Management Systems, an innovative method to monitor management on an animal facility directly from the home cages positioned on the racks.

This method consists on DVC® Lite, composed by three capacitive sensors placed under the cages in order to collect data on the bedding condition, to have information about the probability of an automatic watering system malfunction and, consequently, a leakage detection and to have cages identification through RFID antenna.

In respect of the 3Rs, it avoids losing animals during possible accidents with leakages in the watering systems improving also animals conditions through a direct control of the bedding. This solution also improves the workflow on the management of the animal vivarium reducing the running costs bringing benefits not only for animal health care.

Real time data on the cages are then sent to a scientific cloud-based software developed by Tecniplast, allowing a complete control of the animal's status, transforming raw data into valuable animal activity information.

These results have been reached after numerous tests performed in many laboratories in the world.

In this work all the tests that were performed in Camerino at the Department of Experimental Medicine and Pubblic Health of Unicam are presented.

3.1.2 Data acquisition

The aim of this data set acquisition was to verify the correct output alarm signal of their algorithm when a water flooding happens inside a cage after a malfunction of the Automatic Watering System. Water flooding was simulated in three different cages at the same time using a water container positioned in a highest position with respect to the cages under observation, in order to have a constant water flux. Two different water flows, fast at 3 ml/min and slow at 1 ml/min, were controlled by a tap on the external water container.

The alarm signal generated by the PC directly controls the activation of an electrovalves box to immediatly block the water flooding warning the vivarium's operators about the problem.

Materials and Methods

Data were acquired on the room 26 of the Unicam's vivarium. Room has been set up with one Tecniplast GM80®single side rack installed with Edstrom Automatic Watering System powered by a water tank. A Smart Flow®ventilation unit supplies the air intake inside all the 80 cage positions with 75 ACH and -20% ventilation parameters.

To collect data a Master mini PC DVC with 4 input channels loaded with a Tecniplast custom operating system based on Linux and communicating via Ethernet was used.

In each of the 80 cage positions a DVC®Lite device connected by cable via CAN-bus serial standard to the input channel of the Master mini PC was mounted. The output signal from the Master mini PC controls then the electrovalves box.

Data were taken from 69 CD1 mice and 6 C57BL/6 mice randomly distributed in 64 rack positions. The upper two lines were left empty. Mice were housed on standard GM500 cages under a normal 12hr-12hr light-dark cycle at a controlled temperature of $22°C$.

Three different kinds of litters for bedding to collect different signal from different bedding situation during water flooding were used; ALPHA-dri®, made from alpha cellulose, Corn-cob and Scobis-Uno®, a dust-free wooden litter.

The rack was set randomly following the previous disposition in order to obtain the best statistical variation between variables (3.1).

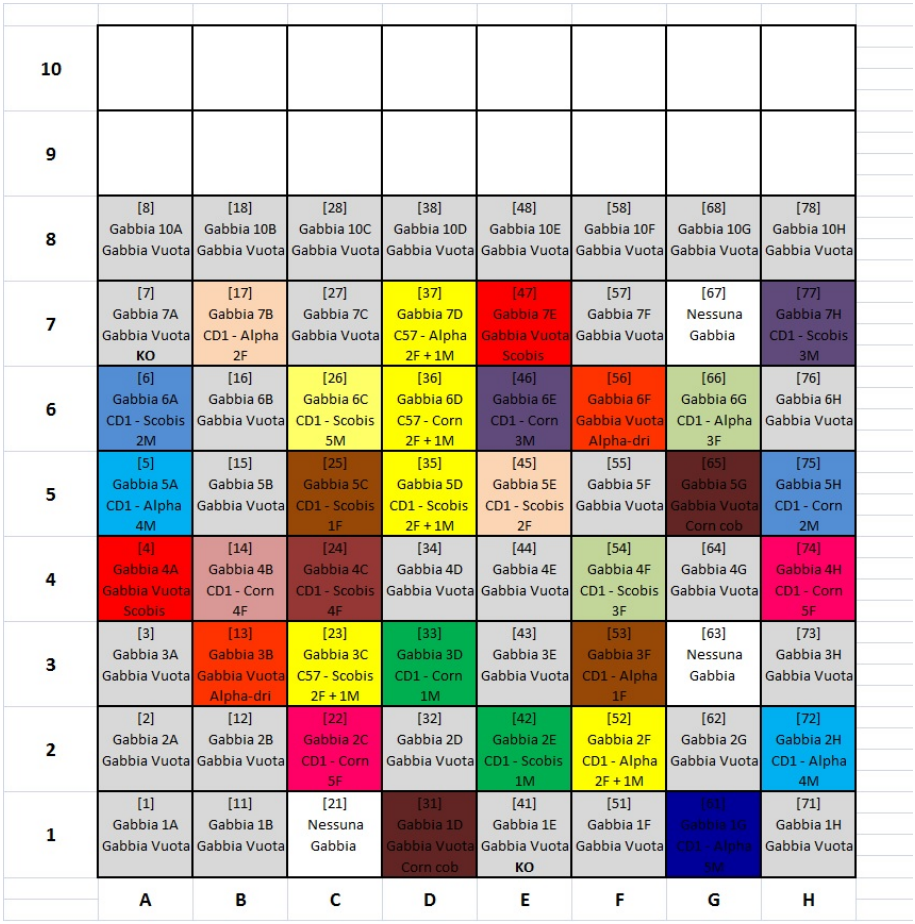

Figure 3.1: Rack disposition on DVC®Lite test. Different number of animals and litters were disposed randomly in the rack in order to obtain the maximum possible variability. Empty cages from animals or litters were used as control for a baseline on the output signal. Empty spaces in the rack were used as calibration signals.

3.1.3 Data analysis on Quantide algorithm results

This algorithm has been provided to Tecniplast by Quantide, a company specialized in IT services. It was developed on the basis of previous data on the DVC®Lite collected in other research labs. Essentially, it is based on a trend-following indicator of economic markets called MACD (Moving Average Convergence-Divergence). Here, only the basic principles of the algorithm are reported.

In financial terms, the MACD indicator shows the relationship between two moving averages of a security's price. In this purpose this indicator was used as a comparative threshold to generate an alarm signal when the electrodes readout data detects a water leakage. MACD indicator is a sort of moving average signal calculated from the difference between two exponential moving averages (EMA) (3.1), a slow one and a fast one. To calculate the fast exponential moving average a short time period is taken as a reference with respect to the slow exponential moving average in which a long time period is considered. This creates a signal that is, in some way, an information on the divergence or convergence of the two original signals. So, calculating the MACD indicator for a precise period of time, depending on what kind of resolution is needed for the purpose, it is obtained a value that is then normalized to a range between 0 and 1.

$$\begin{gathered} Signal_{MACD} = EMA(EMA_{slow} - EMA_{fast}) \\ 0 \leq Signal_{MACD} \leq 1 \end{gathered} \tag{3.1}$$

Four different thresholds are then compared to the value obtained, they represents four alarm levels: green (ok), yellow (warning), orange (danger) and red (water leakage detected).

Results

Algorithm was tested using R, the programming language and environment for statistical computing. Results were then plotted using OriginLab software.

In Fig.3.2 graphs, an alarm signal was detected during a water leakage simulated in the home cage in presence of mice. In raw data represented by the two upper graphs of Fig.3.2, it is possible to note how the animals activity inside the cages introduces noise at the signal, making it difficult to extract the exact information on the leaks moment. But in these cases algorithm worked well.

In particular cases (Fig.3.3), the algorithm completely missed the flooding in the cages. This occurred due to the bad condition of the litter for the first case and due to the slow flooding rate for the second case. With the result that the alarm signal has not been generated.

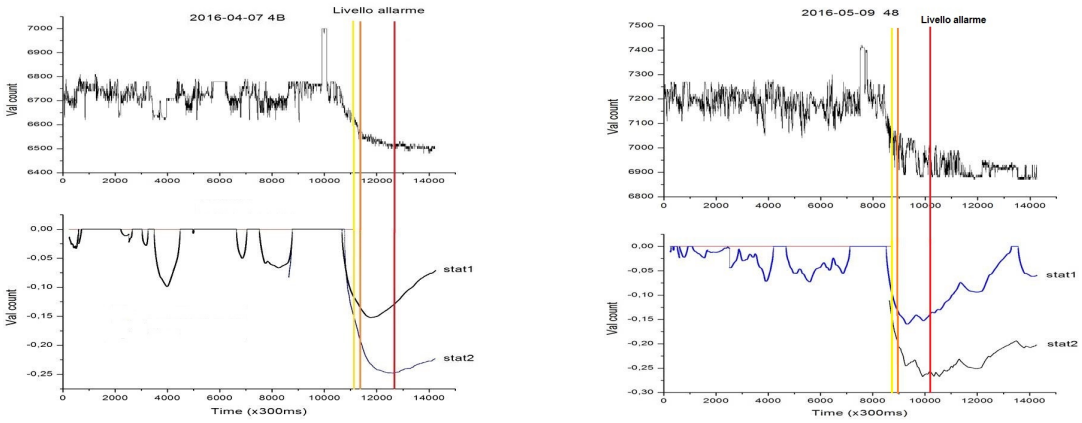

Figure 3.2: Graphs of a water leakage detected by the algorithm. The upper signal in the graphs represents raw output data. The lower signal represents the two indicators STAT1 and STAT2 derived from Eq.3.1. Vertical lines represent the alarm levels. In this case the water leakage was detected due to the increasing divergence of the indicators and consequently to exceeding the relative alarm threshold.

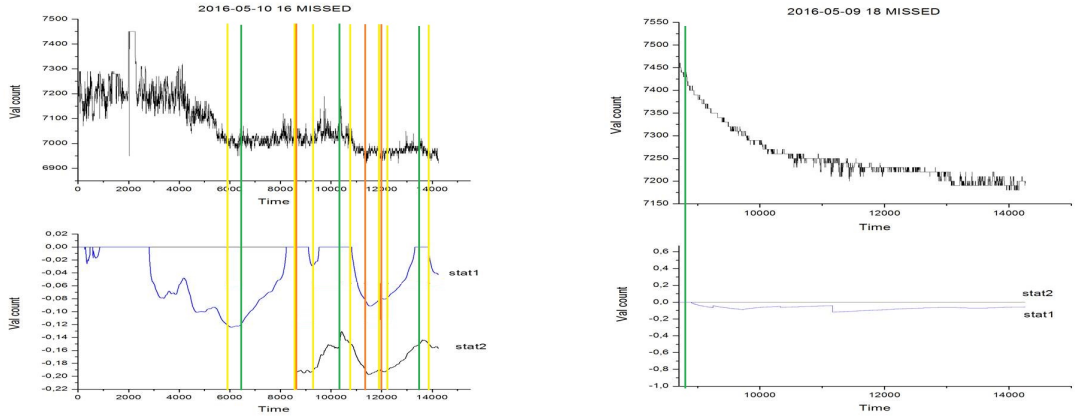

Figure 3.3: Graphs of missed alarm signal by the algorithm on simulated water leakage. The left graph shows a bouncing of the warning and danger signals due to the bad condition of the litter. Flooding has not been reported. The right graph shows a slow water flood just few minutes after starting acquisition. In this case the alarm signal has never been generated.

Conclusions

In conclusion it was possible to report that the algorithm worked well for standard conditions of operation, with a good response also for noisy redout signal as you can see from the previous graph. But for non-standard conditions such as a very dirty litter or for a slow flooding rate the algorithm could have some problems to generate an alarm signal to prevent a leakage on the automatic watering system.

These results allowed Tecniplast to improve the response of their product improving the algorithm in these particular conditions of operation.

3.2 DVC® Big Plate

3.2.1 Introduction

The DVC® Big Plate was created on the basis of the Tecniplast DVC®Lite in order to have a complete platform of analysis over the whole bottom cage. It is composed of 12 capacitive electrodes, disposed in a 4x3 matrix, and it occupies all the physical space under the cage. In this case the analysis algorithm was developed by Tecniplast on the basis of previous results.

A first test was done to verify the correct working operation as it was done for the DVC®Lite. The capability of the system to detect leakage directly from the bottle analyzing the signal coming from the central electrodes was tested too.

In this section all the tests that were performed in Camerino at the Department of Experimental Medicine and Pubblic Health of Unicam are presented.

3.2.2 Data acquisition

The aim of this data set acquisition was to validate the response of the DVC®in its large configuration in order to detect and prevent leakage from the Automatic Watering System and from the bottles used in standard way. Water flooding events were simulated in three different cages at the same time with the same methodologies adopted for the validation test of the DVC®Lite.

Furthermore, water flooding from the bottle position was simulated using a blowpipe connected to a water tank, the flux was regulated by a tap for a constant flood.

The same random configuration for cages position was used in order to obtain the maximum possible variability from the statistical point of view (Fig.3.4).

Materials and Method

Data were acquired on the room 26 of the Unicam's vivarium. Room has been set up with a Tecniplast GM80®single rack installed with Tecniplast Automatic Watering System powered by a water tank.

A Smart Flow®ventilation unit supplies the air intake inside cages with 75 ACH and -20% ventilation parameters. To collect data a Master mini PC DVC with 4 input channels loaded with a Tecniplast operating system based on Linux was used (DVC®Analytics).

The Big Plates were mounted on each position in the rack and connected by cable via CAN-bus serial standard to the input channel of the Master mini PC DVC.

In this case only 13 positions were used to collect data on the cages status in order to reduce the amount of useless data on the basis of previous results. 41 CD1 mice and 20 C57BL/6 mice randomly distributed in the 13 positions were used thus creating a greater concentration of mice housed per cage. This was done in order to increase the degradation of litters during the experiment.

The same litters of the previous tests were used, Corn Cob, Scobis Uno®and ALPHA-dri®.

Results

This test was not performed to validate a new algorithm to detect water floods, so I only collected data on the system in order to have confirmation of the previous results. So, in this test, the results will not be published, but from this dataset Tecniplast could verify the correct operation of the whole system also for the DVC®Big Plate and Analytics.

Starting from this test Tecniplast requested a further test on the locomotor activity inside cages positioned on their DVC®, in order to obtain scientific valuable informations about animal activity inside home-cages, as requested from the 3R's tenets in matter of animal less stressful experiments.

For this purpose it has been proposed a camparative test between the most used systems in locomotor activity acquisition, the Open Field test (Med Associates) and a Video Tracking (Noldus).

	A	B	C	D	E	F	G	H
10								
9								
8	[8] Gabbia 10A Gabbia Vuota	[18] Gabbia 10B Gabbia Vuota	[28] Gabbia 10C Gabbia Vuota	[38] Gabbia 10D Gabbia Vuota	[48] Gabbia 10E Gabbia Vuota	[58] Gabbia 10F Gabbia Vuota	[68] Gabbia 10G Gabbia Vuota	[78] Gabbia 10H Gabbia Vuota
7	[7] Gabbia 7A Gabbia Vuota	[17] Gabbia 7B Gabbia Vuota	[27] Gabbia 7C Gabbia Vuota	[37] Gabbia 7D Gabbia Vuota	[47] Gabbia 7E Gabbia Vuota	[57] Gabbia 7F Gabbia Vuota	[67] Gabbia 7G Gabbia Vuota	[77] Gabbia 7H Gabbia Vuota
6	[6] Gabbia 6A Gabbia Vuota	[16] Gabbia 6B CD1 - Alpha 4M	[26] Gabbia 6C Gabbia Vuota	[36] Gabbia 6D C57 - Corn 2F + 1M	[46] Gabbia 6E Gabbia Vuota	[56] Gabbia 6F C57 - Alpha 4F	[66] Gabbia 6G Gabbia Vuota	[76] Gabbia 6H Gabbia Vuota
5	[5] Gabbia 5A CD1 - Corn 4F	[15] Gabbia 5B Gabbia Vuota	[25] Gabbia 5C CD1 - Scobis 2F + 1M	[35] Gabbia 5D Gabbia Vuota	[45] Gabbia 5E CD1 - Scobis 4M	[55] Gabbia 5F Gabbia Vuota	[65] Gabbia 5G CD1 - Corn 5F	[75] Gabbia 5H Gabbia Vuota
4	[4] Gabbia 4A Gabbia Vuota	[14] Gabbia 4B CD1 - Scobis 5F	[24] Gabbia 4C Gabbia Vuota	[34] Gabbia 4D Gabbia Vuota	[44] Gabbia 4E CD1 - Alpha 2F + 1M	[54] Gabbia 4F CD1 - Alpha 5M	[64] Gabbia 4G Gabbia Vuota	[74] Gabbia 4H Gabbia Vuota
3	[3] Gabbia 3A Gabbia Vuota	[13] Gabbia 3B Gabbia Vuota	[23] Gabbia 3C C57 - Alpha 2F + 1M	[33] Gabbia 3D C57 - Alpha 5F	[43] Gabbia 3E Gabbia Vuota	[53] Gabbia 3F Gabbia Vuota	[63] Gabbia 3G C57- Scobis 5M	[73] Gabbia 3H Gabbia Vuota
2	[2] Gabbia 2A Gabbia Vuota	[12] Gabbia 2B Gabbia Vuota	[22] Gabbia 2C Gabbia Vuota	[32] Gabbia 2D Gabbia Vuota	[42] Gabbia 2E Gabbia Vuota	[52] Gabbia 2F Gabbia Vuota	[62] Gabbia 2G Gabbia Vuota	[72] Gabbia 2H Gabbia Vuota
1	[1] Gabbia 1A Gabbia Vuota	[11] Gabbia 1B Gabbia Vuota	[21] Gabbia 1C Gabbia Vuota	[31] Gabbia 1D Gabbia Vuota	[41] Gabbia 1E Gabbia Vuota	[51] Gabbia 1F Gabbia Vuota	[61] Gabbia 1G Gabbia Vuota	[71] Gabbia 1H Gabbia Vuota

Figure 3.4: Rack disposition on DVC®Big Plate test. Different number of animals and litters were disposed randomly on the rack in order to obtain the maximum possible variability. Empty cages from animals or litters were used as control for a baseline on the output signal. Empty spaces on the rack were used as calibration signals.

3.3 Comparative Tests on DVC®Big Plate

3.3.1 Open Field, Video Tracking and DVC®

To validate the DVC®system, a comparative test was performed between the Tecniplast apparatus, an Open Field maze Med Associates apparatus and a Noldus EthoVision XT Video Tracking system.

The Med Associates Open Field maze is one of the most commonly used platforms to measure behaviors in animal models. It is a fast and relatively easy test that provides a variety of behavioral information ranging from general ambulatory ability to data regarding the emotionality of the subject animal.

The Noldus EthoVision XT Video Tracking system is a software platform that collects video data from one or more cameras. EthoVision XT is used in a wide range of fields, mostly related to neurosciences, such as psychopharmacology, drug discovery, behavioral neurosciences, but also in applied ethology, and animal welfare studies. Here the arenas could be selected by software creating a solution to fit many kinds of experiment protocols, such as Open Field, Morris Water maze, Novel Object Recognition etc.

The three systems are extremely different from the technology point of view, indeed, the Tecniplast one uses capacitive sensing technology, Med Associates Open Field is based on infrared beams breaking inside a dedicated arena with standard dimensions for rats or mice and EthoVision Video Tracking uses image processing from changing pixels value on video data collected by a CCD camera. We can calculate the maximum resolution and sensitivity of the different equipment used. Open Field collects a count every time an animal breaks an IR beam disposed as a matrix inside the arena, this matrix creates 'boxes' of 2x2 cm, so the maximum resolution for this apparatus is a movement of 2 cm in each direction. DVC®collects data from 12 capacitive electrodes under the cage disposed at a distance of $\sim$1 cm each one, if a mouse enters in an electrode area the system could detects his movement, but not with a spacially variation in this area, thus electrodes can detect or not detect the mouse, this gives a low resolution to the instrument readout. EthoVision XT collects data from a CCD camera at 25 fps, this means a resolution in time of about $\sim$40 ms, considering standard velocity of a mouse movement, this tool gives the maximum resolution between the three.

Another big first difference between the available commercial systems and DVC®is that data are collected from animals activity directly inside their home-cages, instead of an unfamiliar environment like that proposed by the other two systems. This means that the habituation time needed for an experiment on locomotor activity is extremely low or totally absent, obviously it depends on the type of experiment.

However, DVC®was not created to replace the standard protocols for locomotor activity recording, but with this system you can increase the quantity of scientific information about that in a familiar environment for the rodent.

Indeed, an home-cage housed rodent behavior is totally different from a new environment behavior. As said in the first chapter, we know that this could introduce stress and anxiety on the animals due to neophobia states.

So, from this test we don't want only to validate the entire Tecniplast system to compare with detection of that parameters that characterize locomotor activity, such as average velocity, resting time or distance travelled, but we expect also to see something correlated to the environment used to perform the test.

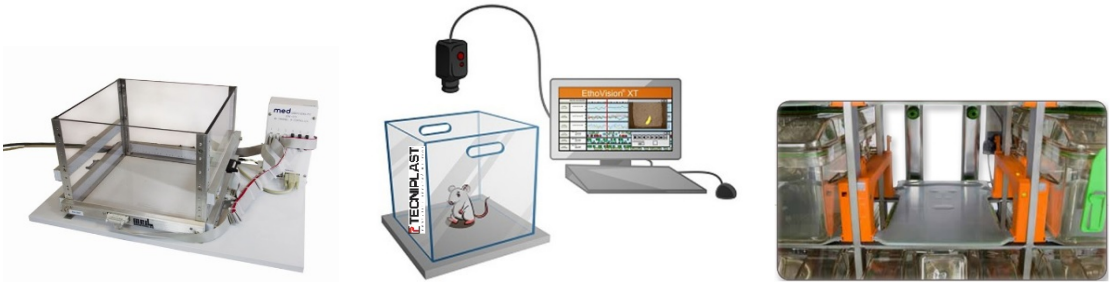

Figure 3.5: The three comparative methods for locomotor activity acquisition.
Left: Med Associates Open Field with IR beam breaking technology.
Center: EthoVision XT Video Tracking on Tecniplast cage.
Right: DVC®Big Plate mounted in a Tecniplast GM80®rack.

Materials and Methods

Data were acquired at the Unicam's vivarium at room 26, for the DVC®, and 51-49 for the Noldus EthoVision XT and Open Field. Room 26 was setup with a Tecniplast GM80®single rack and a Smart Flow®unit. On the rack 5 positions were mounted without Automatic Watering System spouts in order to deprive home-cages from any distraction deriving from water or food intake. In the positions above (Fig.3.6), 5 Video Recording System, each one composed by a Raspberry Pi, a camera module, IR illuminators and a Wi-Fi module, in order to have a real time control of the experiment also for Tecniplast from a Virtual Private Network were setup.

To collect data from the DVC®sensor plates a Master mini PC DVC connected by cable via CAN-bus serial standard protocol to the input channel was used. Video files were collected by Wi-Fi through an Embedded PC and then saved to a NAS storage system.

Figure 3.6: Video recording system on rack and DVC®Big Plate sensor.

In the room 49 was setup the Med Associates Open Field apparatus (Fig.3.5) and in the room 51 the Noldus EthoVision XT Video Tracking system using Tecniplast home-cage as arena.

Tests were performed on 60 mice CD1, 20 mice for each apparatus, during the daytime. The timeline protocol used was the first two days of habituation in which animals are injected with saline and positioned on the apparatus to test for 10 minutes, as habituation, and then for 30 minutes, as test.

At the third day they were divided in two groups, a vehicle control group and a treated group, the time spent on the apparatus was the same of the habituation period.

The vehicle control group were injected with saline. The treated group was injected with cocaine at a dose of 10 mg/kg.

Results

This test was performed in very different conditions, this means that we can not obtain a perfect comparison on data. However, it is possible to fix some important aspects, such as the resolution on motion that is greater on Video Tracking and Open Field, and the environment that is totally familiar on the DVC®(Fig3.7). Graphs and analysis were provided by Tecniplast.

	Open Field	EthoVisonXT	DVC
Technology	IR beam	CCD camera	Capacitive sensing
Resolution on motion	2x2 cm	< 0.5 cm	> 2 cm
Arena dimension	50x50 cm	home-cage	home-cage
Environment	unfamiliar	unfamiliar	familiar

Figure 3.7: Main differences between the three apparatus.

Therefore, the aim of this test is to validate DVC®system on locomotor activity detection and to recognize psychostimulants administration in a familiar environment.

Average velocity results

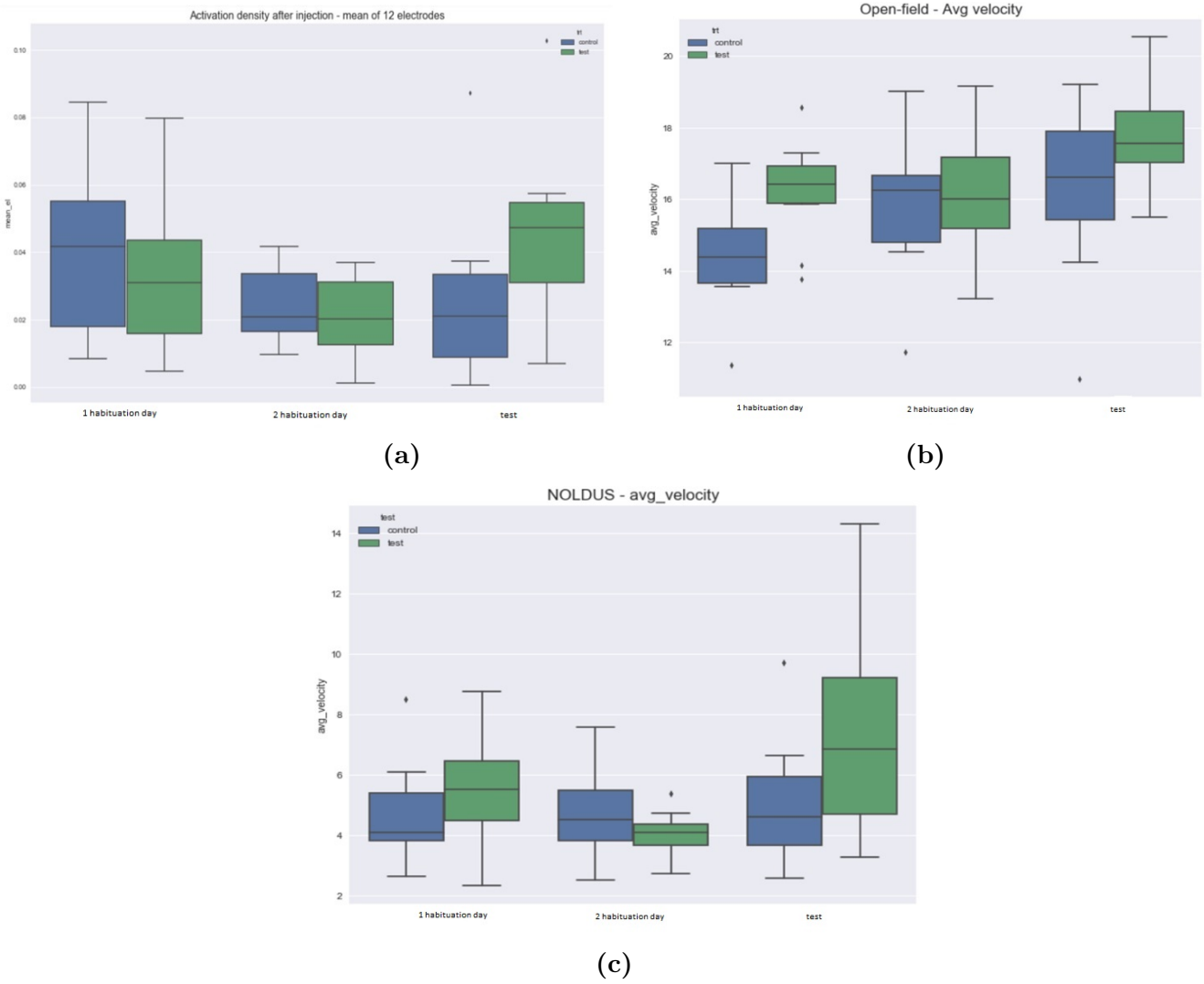

Figure 3.8: [Tecniplast] Results on the three days of experiment **(a)** DVC electrodes activation density results. **(b)** Open Field average velocity results in cm/sec. **(c)** Noldus EthoVision XT Video tracking average velocity results in cm/sec

Open Field and EthoVision XT average velocity data are expressed in *cm/sec*. DVC®data are expressed in activation density indicator, that is a mean of the 12 capacitive electrodes perturbation. This indicator gives an idea of the average velocity of mice into the home-cage, as we can see from 3.8.

On the test data we performed a T-test for each apparatus obtaining these results:

T-test	DVC	Open Field	Noldus
p-value	0.1	0.11	0.06

On the DVC®data we performed also a Kruskal-Wallis test resulting in a p-value = 0.49.

Travelled distance results

On the test data we performed a T-test for each apparatus obtaining these results:

T-test	DVC	Open Field	Noldus
p-value	0.009	0.001	0.04

On the DVC®data we performed also a Kruskal-Wallis test resulting in a p-value = 0.01.

From DVC®data, dividing the total time spent on the test (30 min) in time blocks of 5 minutes each one, we generated time distribution graphs both for activation density and travelled distance (Fig.3.10).

The same was done with the other apparatus on travelled distance, then data were compared using a normalized parameter.

Conclusions

From average velocity and travelled distance data we saw that it is possible to recognize psychostimulants administration directly from inside home-cages and to compare data with other currently used apparatus. From time distribution data on DVC®(Fig.3.10) the effect of cocaine is clear on the locomotor activity data, it is evident that the divergence between the vehicle control group and the treated group increases during the experiment. The vehicle control group activity decreases in time while the treated group one remains almost constant.

From comparative time distribution data (Fig.3.11) on travelled distance we can see that for the vehicle control group a significative decreasing activity on DVC®occurs, this, probably, due to a less stressful and anxiety status of animals inside a familiar environment.

This results are definitely confirmed by the cumulative distance graphs between Noldus and DVC®in Fig.3.12. Here we have a difference of external environment due to the home-cage not positioned on the rack for the Noldus test, from data we can note that on DVC®mice are quieter than mice on Noldus.

All these data confirm the ability of the Tecniplast system to detect locomotor activity and to recognize cocaine administration inside home-cages, confirming also the ability of the system to provide a less stressful environment to the animals.

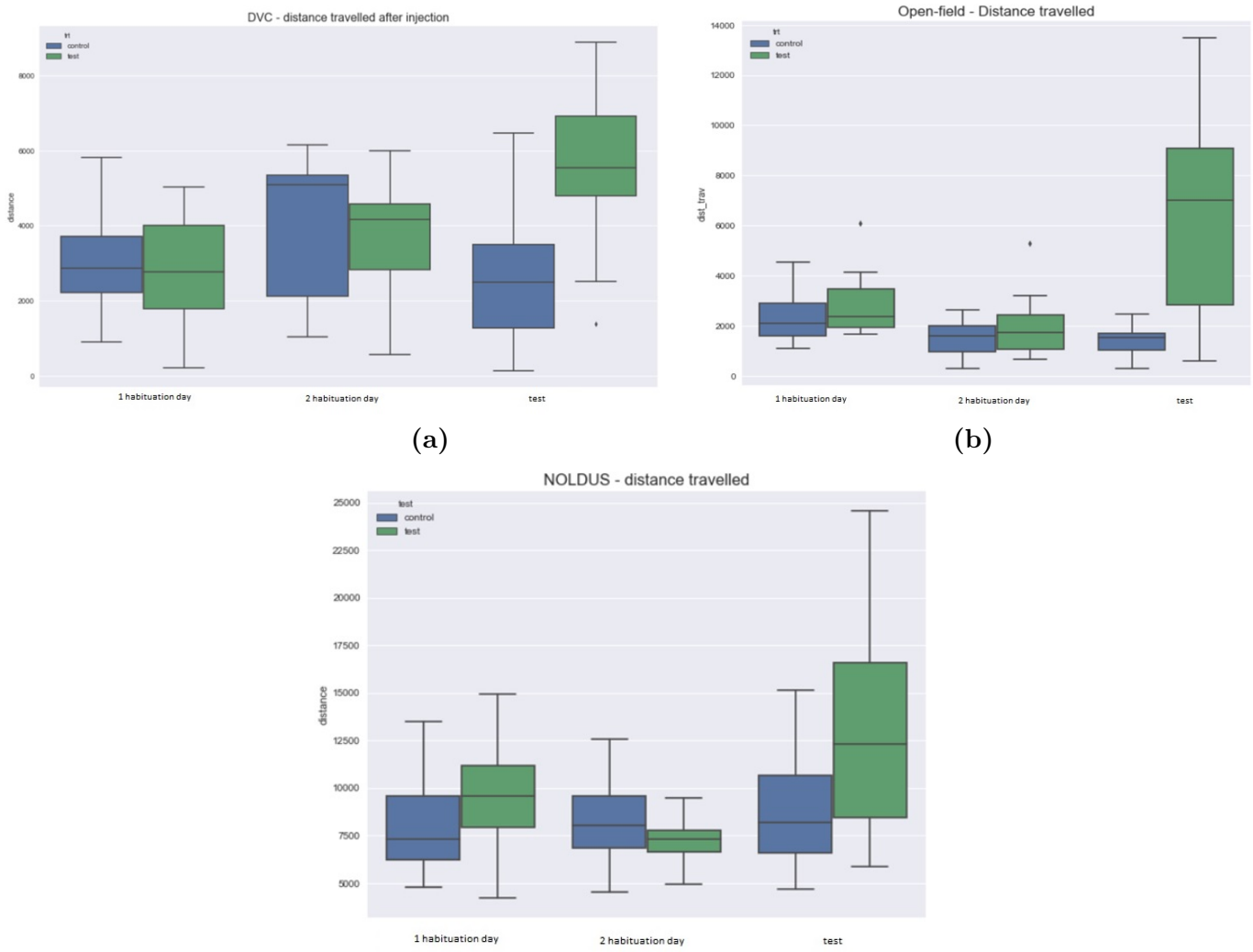

Figure 3.9: [Tecniplast] Results on the three days of experiment **(a)** DVC travelled distance results in cm. **(b)** Open Field travelled distance in cm. **(c)** Noldus EthoVision XT Video tracking travelled distance in cm.

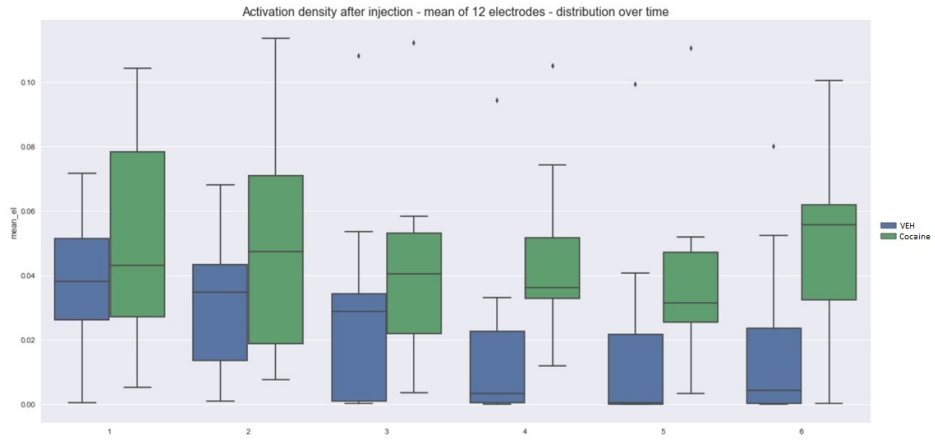

(a)

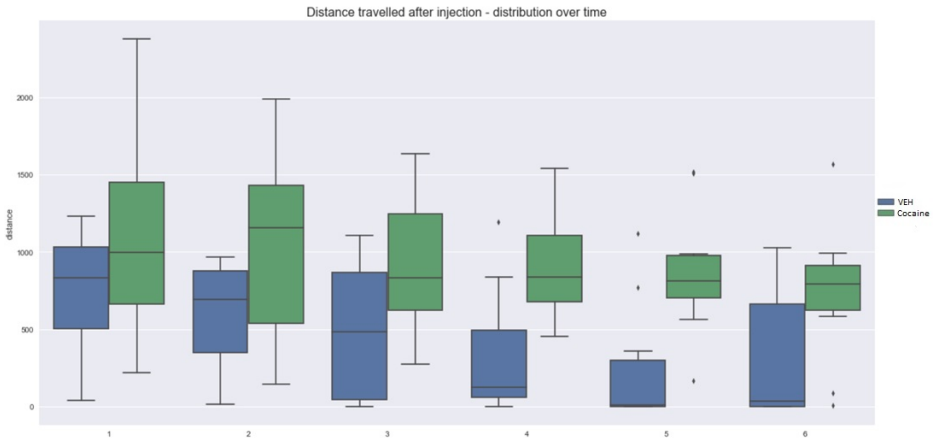

(b)

Figure 3.10: [Tecniplast] Time distribution graphs on DVC **(a)** Activation density time distribution during the whole test on blocks of 5 min. **(b)** Travelled distance time distribution during the whole test on blocks of 5 min.

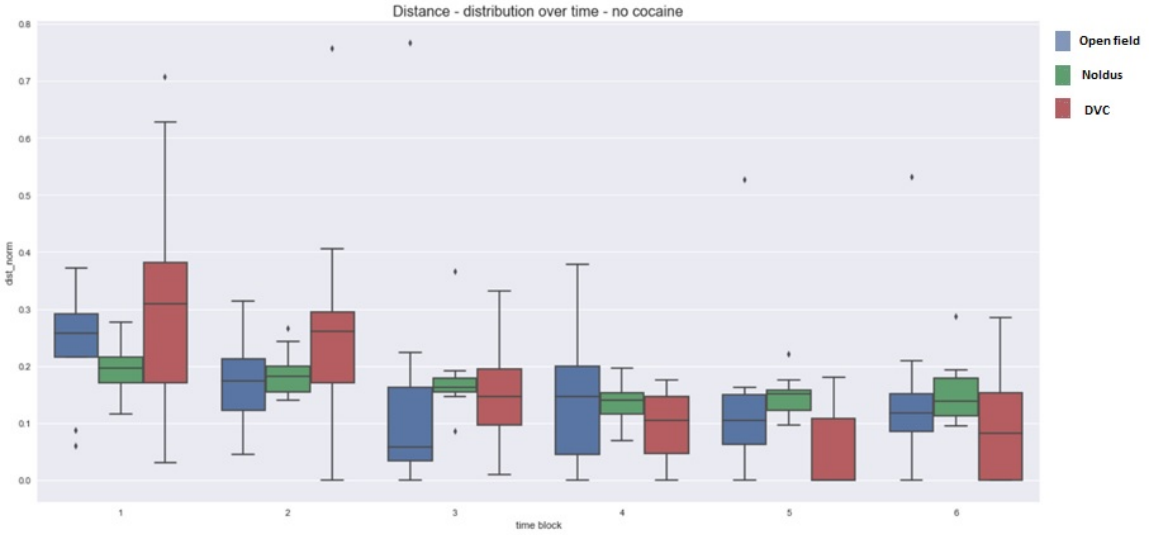

(a)

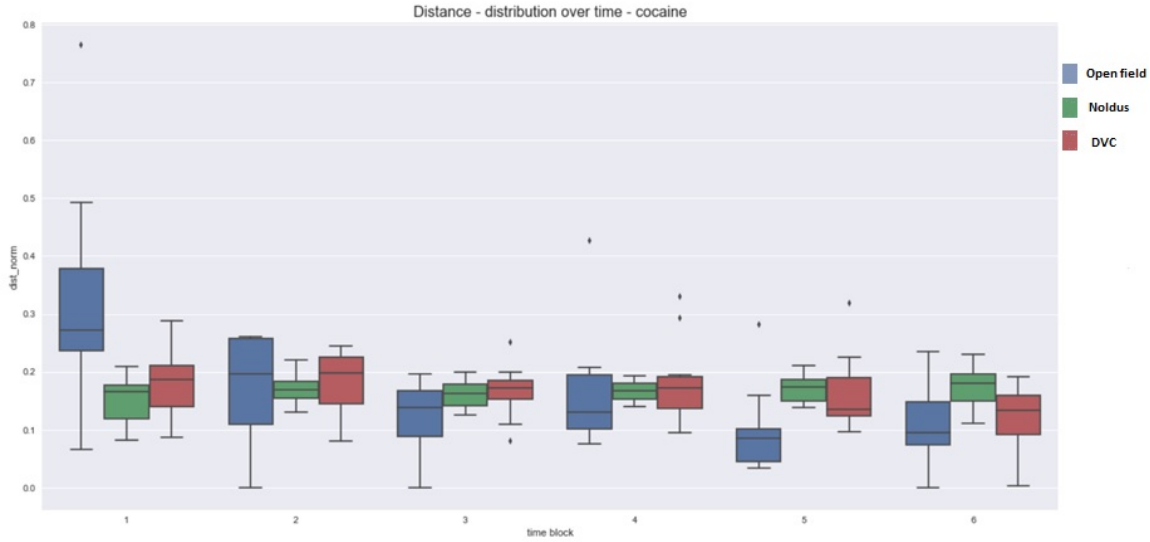

(b)

Figure 3.11: [Tecniplast] Comparison between the three apparatus time distribution graphs on travelled distance **(a)** Travelled distance in each apparatus for vehicle control group. **(b)** Travelled distance in each apparatus for treated group.

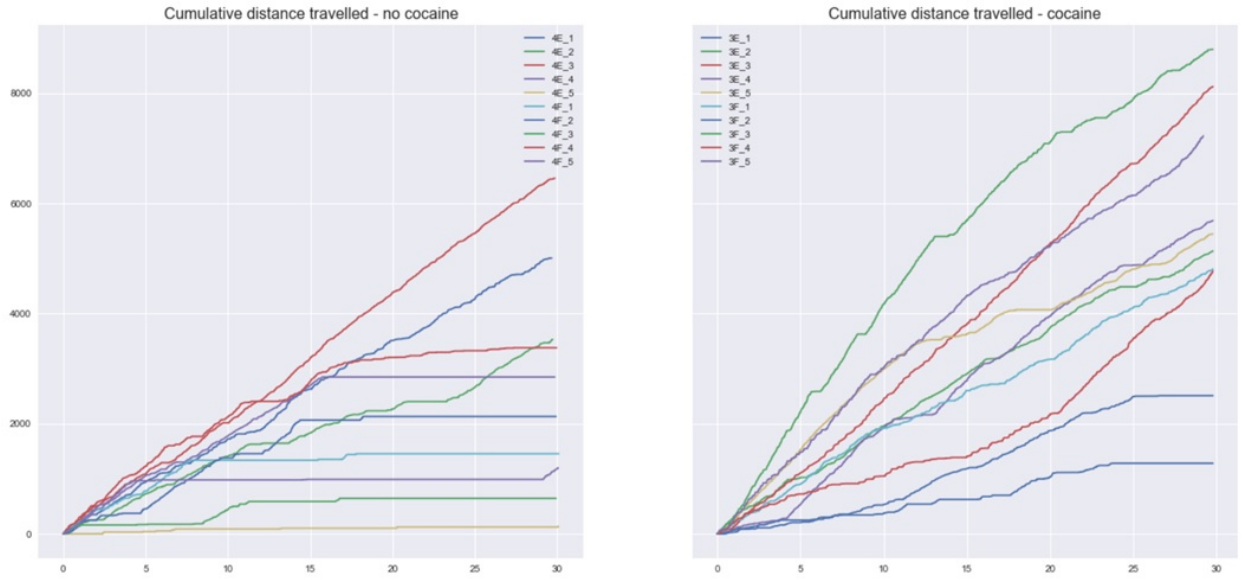

(a)

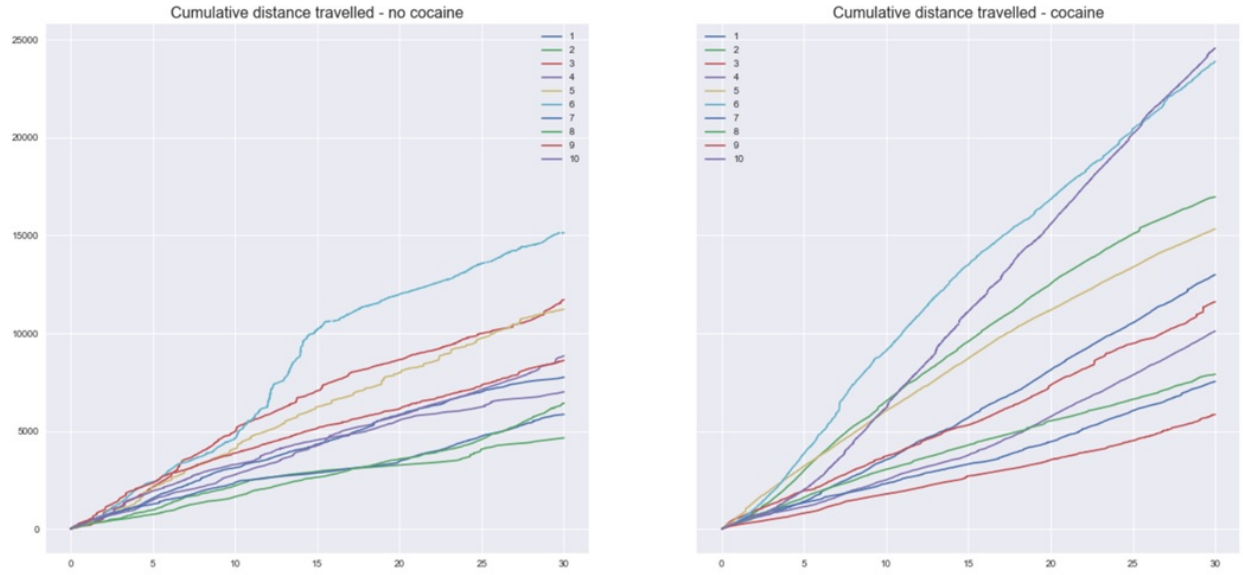

(b)

Figure 3.12: [Tecniplast] Cumulative travelled distance for vehicle control group and treated group **(a)** DVC data for each mouse. **(b)** Noldus EthoVision XT Video tracking data for each mouse.

3.4 USV Microphone

3.4.1 Introduction

Mice, similarly to some other rodent species, communicate with specialized sounds in the ultrasonic range called ultrasonic vocalizations (USV). Evaluation of this behavioral activity enables estimation of the social interactions in animal models such as that used for autistic spectrum disorder, or simply to recognize particular behavior such as dominance, aggression, social play, sexual approaches or a new birth.

Frequencies used by rats and mice to vocalize are extremely differents from ours, in effect their spectrum ranges from 1 kHz to 100 kHz instead human hearing goes from 20 Hz to 20 kHz. The ultrasonic vocalizations emitted by rats and mice have been categorized. There are three main classifications: 22 kHz vocalizations, 40 kHz vocalizations, and 50 kHz vocalizations.

The 22 kHz vocalizations of adults and the 40 kHz vocalizations of pups are emitted in response to aversive situations. For example, isolation, aggression between males, appearance of predators, surprising noises and inescapable foot shocks would elicit these vocalizations. Conversely, the 50 kHz vocalizations emitted by adults are produced during appetitive situations such as social play between juveniles, whilst engaging in mating behaviour, or when the animal is touched gently.

So, having an instrument capable to detect USVs inside an home-cage is important in order to provide further information about the health status of the animals or to detect a new birth and alert vivarium operators.

3.4.2 Methods of implementation and data acquisition

In order to have a good response of the instrument to the ultrasound frequencies, we tested, in collaboration with AM Microsystems, two differents technologies for microphone modules, Electrect and MEMS.

An electrect microphone is a particular capacitor microphone based on an electrect. An electrect is a stable dielectric material with a permanently static electric dipole moment, as the magnetic field generated on a magnet. This eliminates the need for an external polarizing power supply. Usually it needs a preamplifier circuit in order to amplify the low signal level generated.

A MEMS (MicroElectricalMechanical System) microphone is composed by a pressure-sensitive diaphragm etched directly into a silicon wafer by MEMS processing techniques, it is usually accompanied with integrated preamplifier to amplify the signal generated.

Data acquired by these two microphone modules in the room 26 of the Unicam's vivarium were compared with those acquired using a commercial ultrasonic microphone, Avisoft Bioacoustic. Microphones were connected

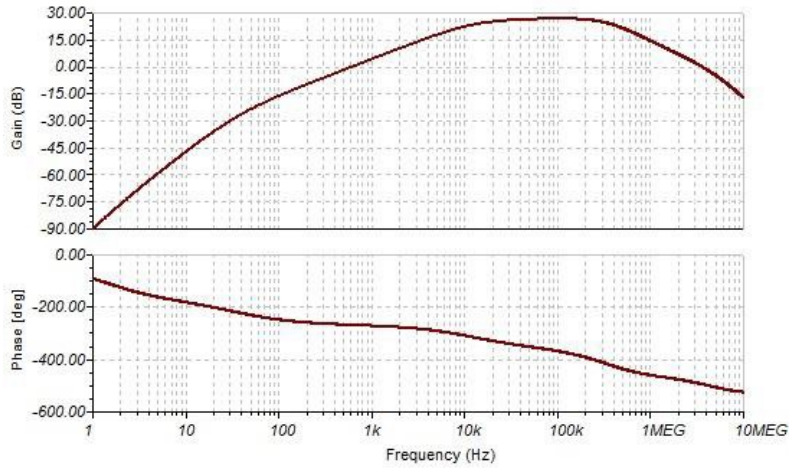

(a)

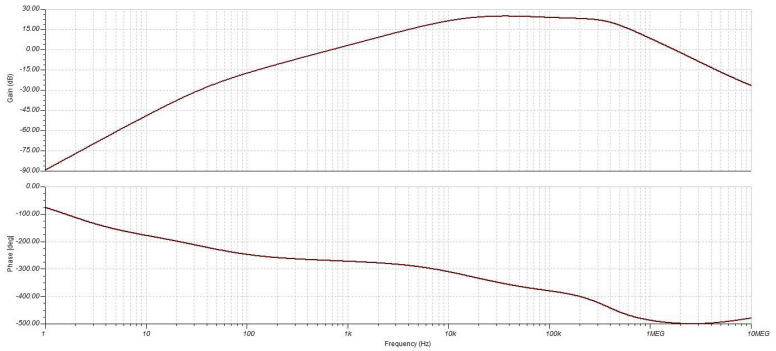

(b)

Figure 3.13: Bode diagrams performed with TINA-TI SPICE-based simulation program **(a)** Electrect microphone simulated frequency response. **(b)** MEMS microphone simulated frequency response.

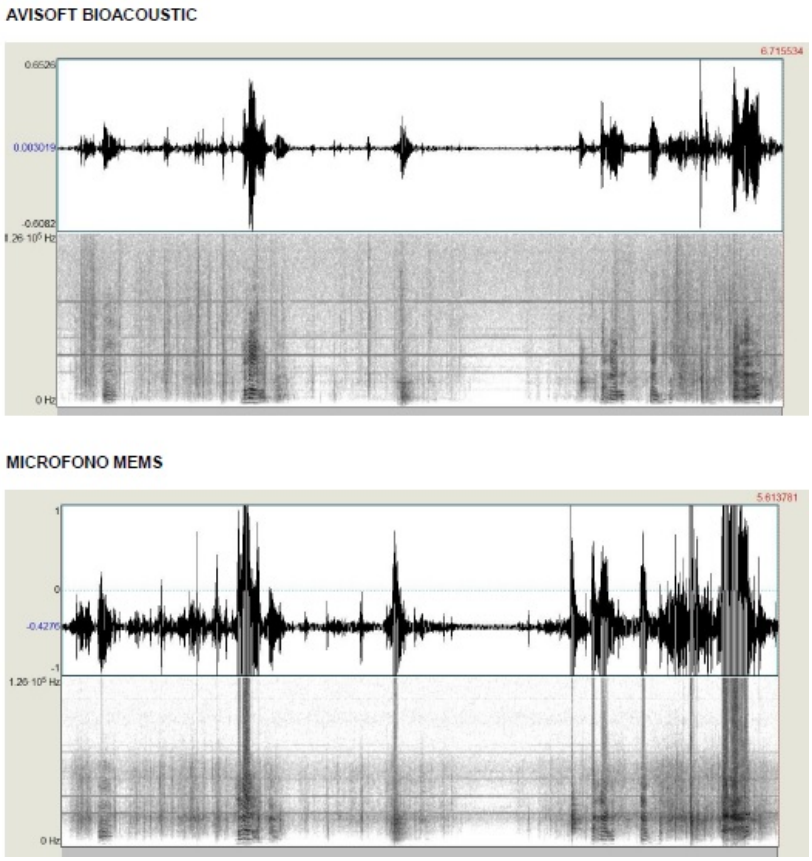

Figure 3.14: Resident vs intruder USV and comparative spectrograms. Waveforms and spectrograms of the Avisoft Bioacoustic microphone and MEMS microphone.

to two preamp circuits with the same topology but adapted to the two different types of microphone to achieve the same tendency on the frequency response, which means increasing gain until 100 kHz (Fig.3.13). Output signal from the preamplifier was acquired through a 16-bit National Instruments acquisition module with a maximum capacity of 250 kS/s.

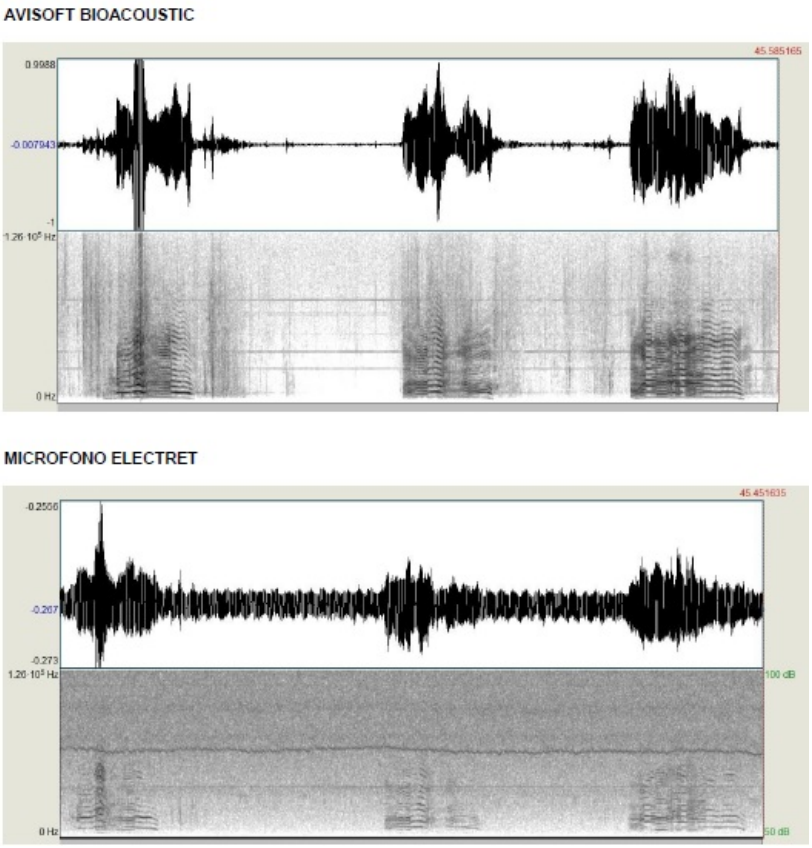

Figure 3.15: Resident vs intruder USV and comparative spectrograms. Waveforms and spectrograms of the Avisoft Bioacoustic microphone and Electrect microphone.

After functionality verification tests of the two circuits with a signal generator, we proceeded to a direct acquisition on mice. Vocalizations were acquired using social defeat techniques, such as resident vs intruder, in which a dominant male was positioned in a home-cage with another dominant male. Mice used were adults CD1. Signals acquired were then compared with a commercial US microphone, Avisoft Bioacoustic. All the instruments were positioned above the cage at the same distance from the animals (∼10 cm). From each acquired signal files .wav were generated through a custom LabView software, they were then analyzed generating the relative spectro-

gram from the original waveform through the application of the Fast Fourier Transform algorithm (FFT). From spectrograms generated (Fig.3.14 and 3.15) it is possible to note that MEMS microphone, at this configuration, remains less sensitive at high frequencies (> 70 kHz) with respect to the Electrect, but it results more stable and with less distortion.

At higher frequencies we can increase the gain of the microphone but with these characteristics we can not improve signal from distortions. For this last reason it was selected MEMS microphone for the purpose.

Improving signal generated from the MEMS microphone for high frequencies, we obtained the following result:

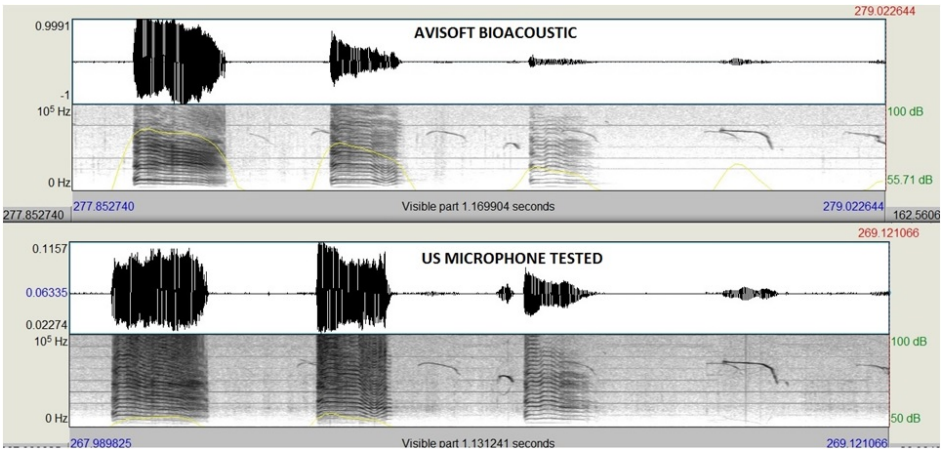

Figure 3.16: CD1 female mouse and pups USV. Waveforms and spectrograms of the Avisoft Bioacoustic microphone and MEMS microphone.

Data from 3.16 were acquired on a female mouse during a birth and already in presence of pups. Pups vocalizations, in this particular situation, are spread over all the spectrum, instead the female mouse vocalizations are centred at ~ 70 kHz. From the comparative spectrograms we can clearly see that there are no significant differences between the microphone responses.

Figure 3.17: Tecniplast microphone module developed from MEMS microphone characterization and validation.

Chapter 4

Optogenetics

4.1 Introduction

Optogenetics is a relative new technique that combines genetic and optical methods to achieve gain or loss of function of well-defined events in specific cells of living tissue, tipically neurons. This field has exploded over the past decade or so and has given rise to great advances in neurosciences. A variety of applications both from the basic and applied research have emerged, turning the early ideas into a powerful paradigm for cell biology, neuroscience and medical research.

Conceptuals inspiration for optogenetics can be traced to the 1970s. In 1979 Francis Crick, taking note of the complexity of the mammalian brain and the fact that electrodes cannot readily distinguish different cell types [17], suggested that a major challenge facing neuroscience was the need to precisely control activity in one cell type while leaving the others unaltered.

At the same time, some microbial single-component light-activated ion pumps were discovered both from bacteria (*Halobacterium halobium*) and from single-cell green algae (*Chlamyodomonas reinhardtii*) which includes membrane-bound ion pumps and channels such as Halorhodopsins [18] or Channelrhodopsins [19].

Wrong ideas of weak and slow photocurrent generated in order to control neurons efficiently or presumption that microbial membrane proteins in fragile mammalian neurons would be poorly expressed or toxic, they were the first preconceptions on the possibility to use these light-sensitive receptor proteins on mammalian brains.

Untill the 2005 [20] it was reported that the introduction of a single-component microbial opsin gene into mammalian neurons resulted in reliable sustained control of millisecond-precision action potentials.

Many other papers appeared over the next years.

From the genetics point of view, new other opsins were developed for differents time kinetics and spectral properties both for activation or inhibition

features (Fig.4.1) allowing different neuronal controls.

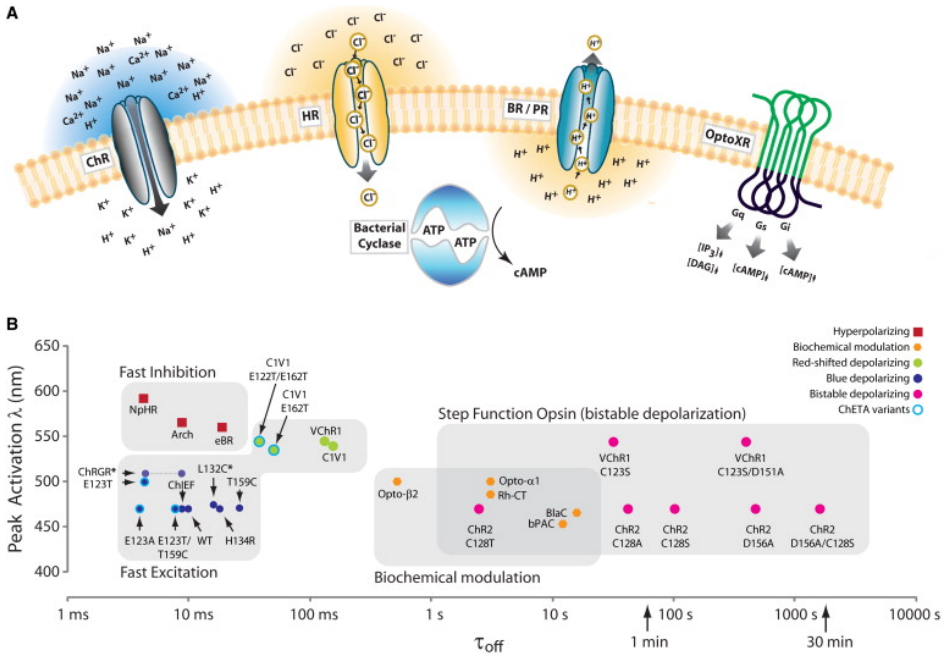

Figure 4.1: Single-component microbial opsin basic properties.
A) Ion channels, ion pump, proton pump and light activated rhodopsin-GPCR chimeras. Transported ions and signaling pathways are indicated. Ion and proton pumps are active proteins phosphorylated with ATP.
B) Kinetics and spectral properties of the main opsins.

In neurosciences, optogenetics allows for the control of specific neurons in living animals and monitoring the effects in real time. It can be used to precisely map brain circuits responsible for a particular behavior, such as fear or drug addiction, and as a therapy for neurological diseases like sleep disorders, epilepsy, psychriatric illnesses such as Alzheimers disease, depression, bipolar, Schizophrenia and Parkinsons disease. Other claims made are to create new memories, the ability to control emotions, the ability to alleviate pain or restore movement in spinal cord injuries and restore sight in the case of a damaged retina.

So, this new technique promises a revolution in the field of brain studies.

4.1.1 How does it work?

Theoretically, optogenetics is a relatively simple mechanism in which, creating a genetic construct, we can obtain any kind of response from any brain areas.

Neurons can be easily controlled using a method that is fast, with responses at the millisecond scale, reversible and cell specific. Furthermore, since different opsins are excited by light at specific wavelengths it is possible to combine several of them in a single animal to perform excitation and inhibition stimulation or for social behavior experiments.

For example, Channelrhodopsin-2 (ChR2) is a blue-light activated (475 nm) cation channel that depolarizes the cell causing the transmission of an action potential. Instead a Halorhodopsin from *Natronomonas* (NpHR) is a yellow-light activated (570 nm) chloride pump that hyperpolarizes the cell preventing transmission of an action potential.

Lentiviral vectors are one of the tools of choice for genetic engineering in optogenetics. Viral vectors take less effort and time than creating transgenic lines. And among them, lentiviral vectors have a larger capacity, which allows including several elements, such as large promoter and reporter genes, in the final construct.

Delivering genes encoding selected opsin through a viral vector allows an expression of that opsin in targeted neurons. Then, light activation through photon absorption of the trans-membrane protein results in neuronal activity and consequently a behavioral observation.

In pharmacology, optogenetics functionality could be compared to that of a medicine or a drug, with the advantage, however, to have an almost instantaneous response and specifically correlated with the brain pathway studied.

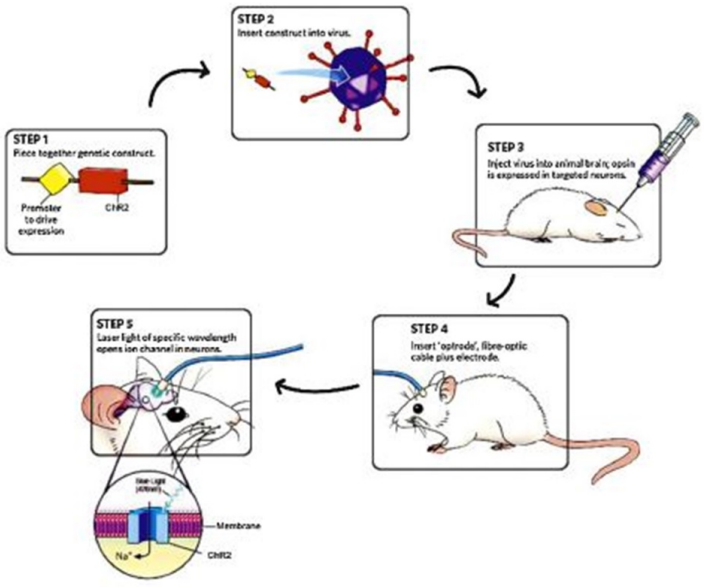

Figure 4.2: Optogenetics procedure.

From Fig.4.2 it is possible to summarize optogenetics procedures in five simple steps.

- STEP 1 - Create a genetic construct based on a photoreceptor;

  A genetic construct is a gene of interest associated with a promoter to drive expression and a photo-sensible trans-membrane protein that will be expressed on the cell membrane.

- STEP 2 - Create a viral vector;

  Viral vectors mediate opsin expression, they are versatile tools for delivering genetic constructs into neurons. Both lentivirus and adeno-associated virus (AAV) vectors have been used to deliver optogenetic constructs into genetically defined cell populations.

- STEP 3 - Inject viral vector;

  Animal will be sedated and the viral vector will be injected in order to obtain an opsin expression in a brain area of interest. Opsin will be expressed in targeted neurons after few weeks.

- STEP 4 - Insert fiber optic cable;

  A fiber optic cable is inserted in the interested area through stereotaxic techniques. Fiber optic carries light from a laser source or an LED directly inside the brain. Different wavelengths means different response on the basis of photoreceptors implanted.

- STEP 5 - Drive a specific wavelength light;

  A square wave light stimulation is driven with a particular frequency and a time duration of the high impulse into the interested brain area. Frequency and high impulses are generated depending on what kind of neurons are targeted and what kind of behavioral response is requested.

From some points of view this approach is the best for a good result in optogenetics experiments, but in other respect this is not the best way to go about it.

One of the most important problems with this approach is the relative impossibility of social interaction experiments implementation due to the presence of a fiber optic cable connected to the head of each animals. Fiber optic cables could be a physical constraints in an operant conditioning cage.

Furthermore, in many cases, laser light optical power could damage neurons and organic tissue through an important increasing in temperature around the interested brain area due to scattering and absorption effects.

Of particular concern is the potential for heat induced by prolonged optical stimulation, elevating neurons firing rate locally even in absence of opsin expression [21].

The photocurrent in a neuron resulting from a pulse of light will depend upon many factors, including the properties of the opsin being expressed, the wavelength, intensity and duration of the incident light. In all cases, however, the rate of absorption of photons of a given wavelength is proportional to the local photon flux; that is, the number of photons incident per unit time per unit area. When designing a light delivery system to activate rhodopsins, it is therefore primarily this parameter that we want to measure and control.

Optical power on the fiber optic tip, however, must reach at least the opsin activation threshold, for Channelrhodopsin-2 this is $\sim 1\ mW/mm^2$, and it must not exceed $\sim 100\ mW/mm^2$ in order to avoid a permanent damage on neurons struck by the intense light beam. This could cause epileptic states and paralysis on the animals.

For these reasons, in the last few years, research of new techniques to deliver light has grown fast, mostly on wireless and low energy consumption implanted circuits based on high efficiency LEDs.

In these cases the main problem could be the size of the implanted optoelectronic device (Fig.4.3) or the maximum time duration for an experiment due to the small energy capacity of the batteries used.

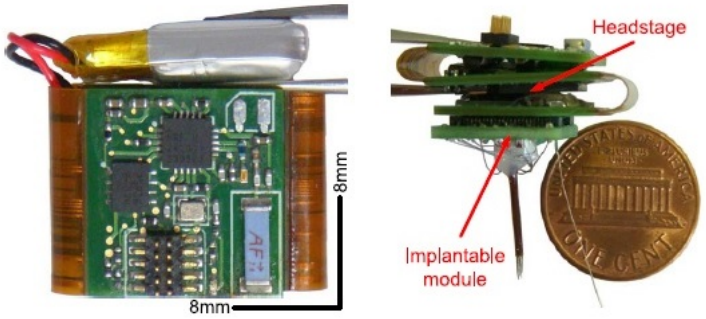

Figure 4.3: Wireless optogenetics and electrophysiological implantable recording device [22]. Size and weight of the entire implantable device shall be such that animals must be free to move.

4.1.2 Optical properties of Brain Tissue

For a given opsin gene, functional expression levels and light power density reaching the expressing cells will together determine the efficacy of light-based control. To estimate this density of light reaching the targeted cells one must consider the propagation of light in tissue.

Light propagation in neuronal tissues can be modeled using different mathematical models. The amount of light transmitted through a biological

tissue depends mainly on light scattering, photon absorption and conical spreading of light from the tip of the implanted light source. Transmission properties also depend on wavelengths used for opsin activation, as a matter of fact a longer wavelength light scatters less than a shorter one and therefore penetrates more deeply.

In order to have a complete knowledge of the optical properties of brain tissues, we need to know also the anisotropy factor map of the area or at least we need to know the scattering coefficient per unit thickness both for mice and rats brain.

So, taking into account illumination of deep brain areas using optical fibers two theoretical models can be used:

- The **Kubelka-Munk** model;
- **Monte-Carlo simulation** methods;

Kubelka-Munk Model

The amount of light transmitted through a slice of brain tissue can be formalized using the Kubelka-Munk theory of light propagation in scattering and absorptive media [23].

This method is based on the idea that light propagates in two opposite directions, the transmitted flux and the scattered flux. The model further assumes that reflection and absorption are constant over the thickness represented by $\hat{z}$ axis.

The relative intensity is calculated then considering both a geometrical decreasing parameter, that is function of geometrical properties of the fiber optic tip, and a transmission fraction depending on the scattering coefficient per unit thickness.

$$\frac{I(\hat{z})}{I_0} = \frac{\rho^2}{(S\hat{z}+1)(\hat{z}+\rho)^2} \tag{4.1}$$

where ρ is the geometrical factor

$$\rho = r\sqrt{\left(\frac{n}{NA}\right)^2 - 1} \tag{4.2}$$

and the transmission fraction is represented by

$$T = \frac{1}{S\hat{z}+1} \tag{4.3}$$

where S is the scattering coefficient.

So, considering S=11.2 mm^{-1} for mouse brain tissue and S=10.3 mm^{-1} for rats, we can calculate the irradiance profile, in terms of relative intensity, for rat brain in function of distance from the tip (Fig.4.4) utilizing parameters used for this final purpose.

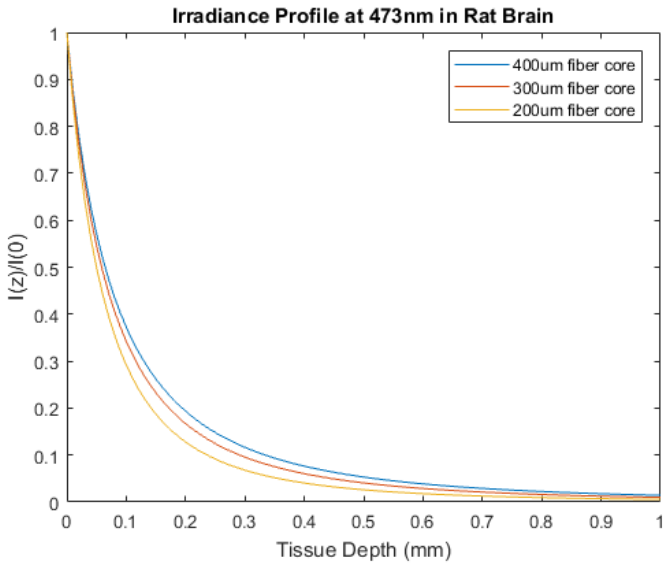

Figure 4.4: Irradiance profile in terms of relative intensity for a rat brain at a wavelength of 473 nm for different values of fiber optic core diameters.

From the graph it is possible to note that for this particular wavelength biological tissues can be considered as an extremely absorptive medium. The simulated intensity profile also indicates that a 473 nm light beam injected in a greater diameter fiber optic core could reach a wider brain tissue depth at the same optical power density generated.

This result could be useful also considering the heat induced by prolonged optical stimulation patterns [21].

This theoretical prediction is in conformity with experimental data found in literature for what concerns light transmission in deep brain.

Monte-Carlo simulation methods

Monte-Carlo methods are a broad class of computational algorithms that rely on repeated random sampling to obtain numerical results. In order to have a simulation of the light distribution and a prediction of light propagation in biological tissues, Monte-Carlo methods track trajectory of each photon, estimated on a random walk, and calculate the light intensity at each position. The accuracy of these methods depends on the number of photons and, consequently, on the trajectories launched.

The first method illustrated is based on Henyey-Greenstein phase function [26]. It consists on dividing the space in a grid of voxel in which photons generated propagate in random directions calculated according to the Henyey-Greenstein function.

The H-G phase function is characterized by the variation of g that is defined as the anisotropy factor (Eq.4.4).

Values of g can range from backscattering to forward scattering, $-1 \leq g \leq 1$. Usually its value is 0.89-0.9 for brain tissue.

$$p(\theta) = \frac{1}{4\pi} \frac{1 - g^2}{(1 + g^2 - 2g\cos\theta)^{3/2}} \tag{4.4}$$

This function is normalized such that the integral over 4π steradians is unity.

$$\int_0^{2\pi} \left\{ \int_0^{\pi} p(\theta) \sin(\theta) d\theta \right\} d\phi = 1 \tag{4.5}$$

We can write it as a function of $\mu = \cos(\theta)$

$$p(\mu) = \frac{1}{2} \frac{1 - g^2}{(1 + g^2 - 2g\mu)^{3/2}} \quad \text{and then} \int_{-1}^{1} p(\mu) d\mu = 1 \tag{4.6}$$

So, forward scattering is for $\theta = 0$, $\mu = 1$, while backscattering is for $\theta = \pi$, $\mu = -1$. In order to use the H-G function for Monte-Carlo simulations, we need the accumulated distribution.

$$\begin{aligned} P(\mu) &= \frac{1}{2} \int_{-1}^{\mu} \frac{(1 - g^2) d\mu}{(1 + g^2 - 2g\mu)^{3/2}} = \\ &= \frac{1 - g^2}{2g} [(1 + g^2 - 2g\mu)^{-1/2} - (1 + g)^{-1}] \end{aligned} \tag{4.7}$$

So, remembering that $\mu = \cos(\theta)$ and chosing randomly the direction of propagation of each photon in function of θ we can calculate the probability density in space. Defining the photon flux Φ as the number of photons per second per unit area we can calculate the optical power density H, expressed in $\frac{W}{m^2}$, as

$$H = \Phi \frac{hc}{\lambda} \tag{4.8}$$

where h is the Planck's constant, c the speed of light and λ the wavelength of the light irradiated (Fig.4.5).

The second Monte-Carlo method illustrated is that used in [24]. A 3D brain atlas was created on the basis of magnetic resonance imaging (MRI) digital database in order to reconstruct the entire brain of a C57BL/6J mouse.

The whole 3D space is then divided in voxels at which different optical properties were assigned in order to obtain a modeled brain tissue.

Photon trajectories are calculated as

$$t = \frac{-\ln(random\#)}{\mu_s} \tag{4.9}$$

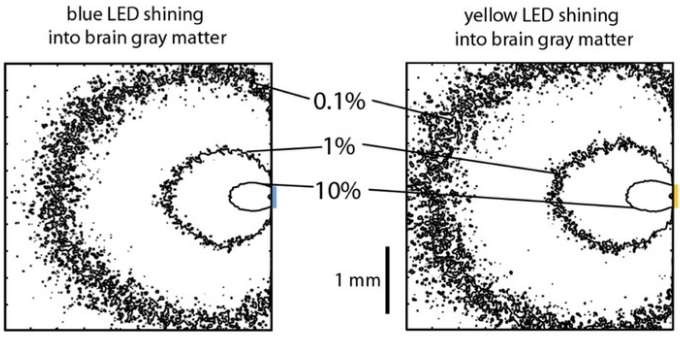

Figure 4.5: Henyey-Greenstein phase function irradiance profile for a blue (left) and yellow (right) light emitters.[Ed Boyden et al.]

where μ_s is defined as the scattering coefficient and *random numbers* were randomly generated.

The scattering coefficient is calculated on the basis of a reduced scattering coefficient μ_{rs} that takes into account the variation of optical properties for what concerns scattering tissue characteristics at different wavelengths. It is then defined as

$$\mu_s = \frac{\mu_{rs}(\lambda)}{1-g} \tag{4.10}$$

where $g = 0.90$ is the anisotropy factor. The reduced scattering coefficient is calculated as

$$\mu_{rs} = a\left(\frac{\lambda}{500[nm]}\right)^{-b} \tag{4.11}$$

in which a is a scaling factor for the reduced scattering coefficient at 500 nm wavelength. The b factor is defined as the scattering power that goes from $\sim$0.5 to $\sim$2 depending on the increasing hardness of the tissues.

The total absorbtion coefficient μ_a is then calculated for each voxel as

$$\mu_a(\lambda) = BS\mu_{a,oxy}(\lambda) + B(1-S)\mu_{a,deoxy}(\lambda) + W\mu_{a,water}(\lambda) \tag{4.12}$$

where S, B and W are respectively the hemoglobin oxygen saturation, the average blood volume fraction and the water content on the tissues.

These parameters were differentiated in respect of gray matter and white matter mapped in a brain anisotropy map calculated from MRI images.

Then a photon weight W is deposited on the voxel for each step depending on photon trajectories t (Eq.4.9) and total absorption coefficient μ_a (Eq.4.12).

$$W = (1 - e^{-\mu_a t}) \tag{4.13}$$

This last Monte-Carlo method was used in the calculation of optical power density, light distribution inside the brain and anisotropy map for my device parameters (Fig.4.8).

4.1.3 3D Monte-Carlo simulation

In order to have a theoretical expectation of a deep brain illumination for my device, I used a 3D Monte-Carlo simulation platform called OptogenSIM performed in MATLAB [24].

This Monte-Carlo method, described above, allows me to validate some features chosen for the development of the optogenetics wireless device, so, I fixed some important parameters such as:

- The chosen area is the Basolateral Amygdala (BLA) which mediates, together with the Nucleus Accumbens, the specific Pavlovian-instrumental transfer for learning behaviors in response to a conditioned stimulus, thus modifying an operant behavior (Fig.4.6).

- The optical power at the tip of the fiber ($\sim 0.9mW$), resulting from the coupling of a high efficiency blue LED ($\sim 4mW$) to an optical system.

- The wavelength centred at 475 nm needed to activate the expressed Channelrhodopsin-2 on BLA neurons.

- The Numerical Aperture (NA=0.39) of the multimode optical fiber.

- The fiber core diameter of 400 μm.

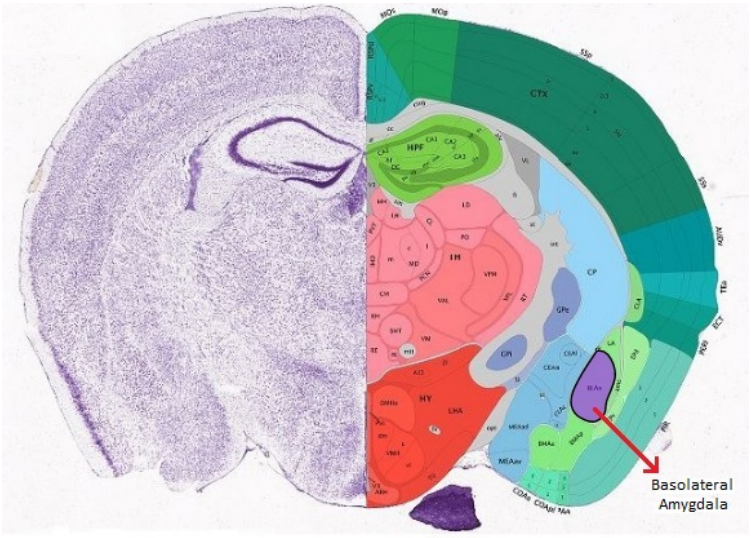

Figure 4.6: Coronal mouse brain slice and Basolateral Amigdala coordinates.

From 4.8 OptogenSIM simulation it is possible to note that using the presented parameters the optical power density for activation threshold of Channelrhodopsin-2, reported as $\sim 1mW/mm^2$, can be reached.

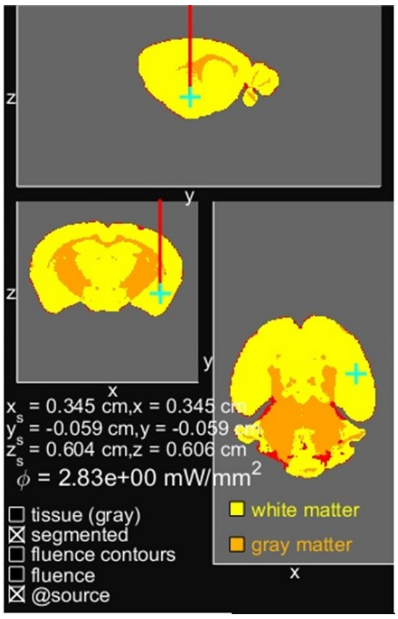

Figure 4.7: Anisotropy factor map for gray matter and white matter in BLA coordinates. Sagittal, coronal and horizontal mouse brain sections.

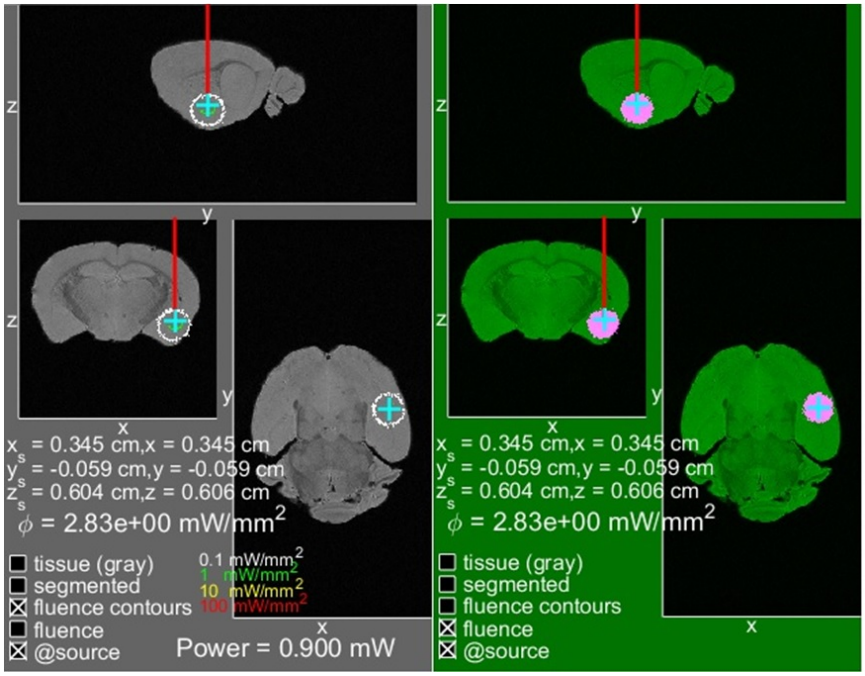

Figure 4.8: Optical power density (left) and light distribution (right) in BLA coordinates. Sagittal, coronal and horizontal mouse brain sections.

4.2 Optical configuration

Optimizing light delivery in deep brain tissues for optogenetics is critical in order to accurately stimulate the neurons of interest while reducing non-specific effects such as tissue heating or photodamage. A long light pulse stimulation could increase action potentials firing rate straining the neuron interested and, consequently, an increasing probability of damage, triggering a cascading effect. In fact, an high firing rate of action potentials leads to a gradual increase of intracellular calcium concentration entering from presynaptic voltage-gated calcium channels. As this calcium concentration rises, it eventually starts a chain reaction which activate the cell's apoptosis pathway. As this rapid firing occurs, this doomed neuron may produce similar overexcitation in downstream neurons. Because the cell was in such a nasty state before it died, this means it will introduce all sorts of dangerous signaling molecules into the immediate area, which can cue the apoptosis pathway in neighboring cells. This phenomenon is called excitotoxicity and it is one of the causes of a stroke.

In order to avoid any kind of photodamage from the optical power injected it is necessary not to exceed the damage threshold of 100 mW/mm^2 from the fiber optic tip to prevent an overstimulation of the neurons due to the presence of the photoreceptors. This means that for a fiber optic core diameter of 400 μm we have to stay below an optical power of 12.5 mW injected from outside. Reducing the fiber optic core diameter this value decrease.

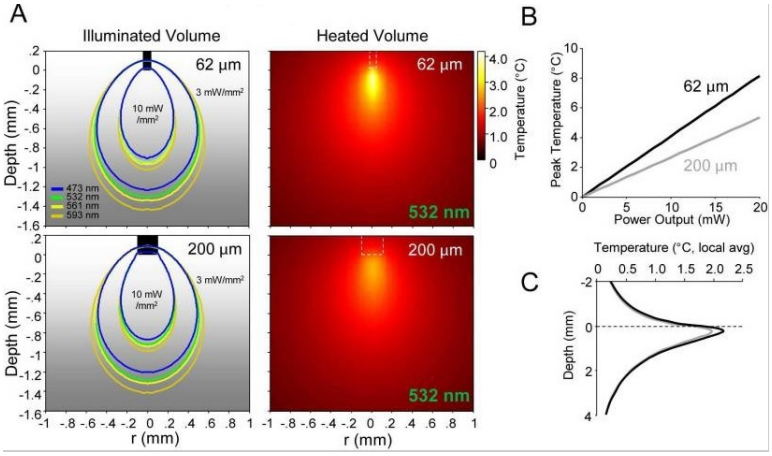

Figure 4.9: Heat induction for different fiber sizes NA = 0.22. **A)**Illuminated volume at different wavelengths and temperature changes for 10 mW/mm^2 optical power density at 532 nm. **B)** Peak temperature change as a function of optical power. **C)** Temperature change as a function of depth.[21]

Usually a laser is coupled directly through the optical system composed essentially from a single fiber optic cable. Obviously, with a laser pulse stimulation we don't have any problem to reach the activation threshold, but, unfortunately, it is also very easy to reach optical power density in deep brain near or above the neuron damage threshold.

At these optical powers it has been demonstrated that heat propagation starts to be a problem [21] for the normal neuronal activity.

4.2.1 Optical parameters

From the datasheet an high efficiency blue LED [27] gives a luminous intensity (I_v) of 65 mcd at a current of 2 mA with a forward voltage of 2.65 V.

Considering also a viewing angle (θ) of 40° for the optical beam we can calculate the optical power (Φ_e) for the LED luminous flux (Φ_v) on the solid angle (Ω).

$$\Phi_e = \frac{I_v \Omega}{683 \cdot 0.1126} \quad \text{for} \quad \Omega = 2\pi[1 - \cos(2\theta)] \tag{4.14}$$

where 683 is the conversion value for lm to W and 0.1126 derived from the photopic luminosity function $\bar{y}(\lambda)$ at 475 nm [28].

From Eq.4.14 it is possible to obtain an optical power for this LED of 4.4 mW.

This optical power must be injected into an optical fiber with minimal optical losses. To obtain an optical configuration with an efficient coupling system I used two ball lenses.

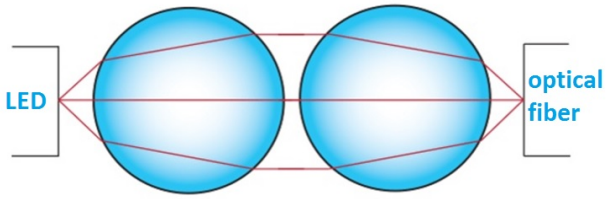

Figure 4.10: Optical configuration for coupling LED to optical fiber.

This configuration allows me to obtain a focused light beam directly on the tip, increasing the power injected on the fiber. Important parameters for ball lenses are the effective focal length (EFL) and back focal length (BFL) depending on the index of refraction of the material [$n(\lambda)$] and the diameter (D) of the spheres.

$$EFL = \frac{n(\lambda)D}{4[n(\lambda) - 1]} \quad \text{and} \quad BFL = EFL - \frac{D}{2} \tag{4.15}$$

The spherical shape of the lenses introduces spherical aberrations on the beam path. The breadth of this problem depends on the index of refraction of the ball lenses and consequently on the selected construction material.

To understand this problem and chose the best material for the lenses I performed a MATLAB calculation on the spherical aberration profile for different materials, with different index of refraction, suggested for the purpose.

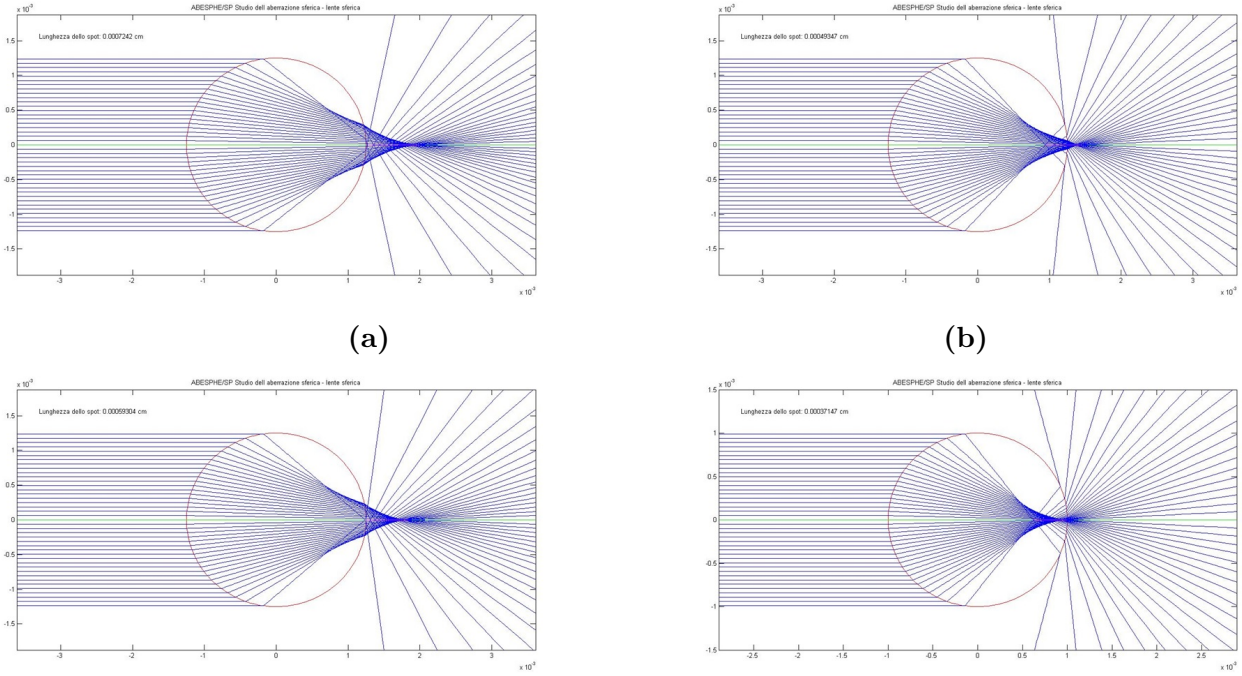

Figure 4.11: Spherical aberration profiles from a 475 nm light source **(a)** Fused Silica. **(b)** Sapphire. **(c)** N-BK7. **(c)** S-LAH79

From data shown in Fig.4.11 it can be seen that the best spherical aberration profile with no internal reflection it is obtained by fused silica ball lenses ($n = 1.46$ at $475nm$). These spheres give a focal point at a distance from the surface of $\sim 0.55\ mm$.

The numerical aperture (NA) of the ball lens must be less than or equal to the NA of the optical fiber in order to couple all of the light. So, for the ball lenses used with a diameter (D) of 2.5 mm and an optical fiber core of 400 μm we have a NA of:

$$NA_{sph} = \frac{2d(1-n)}{nD} = 0.1 \quad \text{and for the fiber} \quad NA_{fib} \geq 0.39 \qquad (4.16)$$

So, calculating the acceptance cone given by the angle θ for the optical fiber in air ($n_0 = 1$) as

$$\theta = \arcsin \frac{NA_{fib}}{n_0} \tag{4.17}$$

We have all the parameters needed to set up a coupled optical system (Fig.4.12). Using a ceramic cannula from Thorlabs and a cylindrical symmetry for the alignment, I obtain an implantable optical system.

Figure 4.12: 3D drawing of the implantable optical system used.

4.3 Electronic circuit

Optogenetic stimulation needs a precise control of frequency, high impulse and time duration of the pulse light emitted in order to avoid all those problems from the biological point of view. At the same time we need also a user friendly system to handle easily from an operator, it should be implantable thus it does not have to weigh more than the 10% of the full weight of the animal and it must be operational at least for the duration of the whole experiment (4-5 hours).

To obtain that we need low power consumption components and a battery that can be used with animals, therefore non-toxic one, in a low dimensions layout.

For this purpose it was chosen a Zn-air battery (Fig.4.13). This battery has a high energy density value of $\sim 20\ MJ/L$ and a specific energy of ~ 1.7 MJ/kg generated by oxidation of zinc with the oxygen normally present in the air through little holes in the metal cap, that makes it a useful candidate for an optogenetics wireless system.

However, Zn-air batteries have a low generated voltage, from available commercial cells usually $\sim$ 1.35-1.4 V, and a high dropout voltage when they are subject to high load current. In order to drive an high efficiency LED it is needed a peak load current of $\sim$ 20 mA during the high impulse of

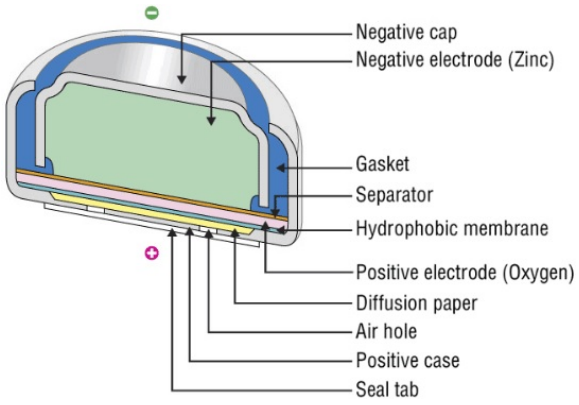

Figure 4.13: Cross section of a Zn-air button cell battery.

the square wave signal for a time duration that may vary depending on the stimulation requested (1 ms to 20 ms). This means that the battery should have a relative high capacity in order to be used during all the experiment. From these parameters I chose an A675P Zn-air battery with the following characteristics: a voltage of 1.4 V, a capacity of 500 mAh and a maximum available current of 30 mA. To have a precise control of the system and a good managing of battery supply charge it is needed a microcontroller with an integrated boost converter in order to step up the low battery voltage at least at 3 V to feed both the microcontroller itself, the LED and a low energy consumption preamplifier circuit to have an infrared remote control of the entire system. For the purpose the selected microcontroller was the ATtiny43U, a 8-bit AVR microcontroller with 4 kB in-system programmable flash and integrated boost converter. For the remote control of the system was selected the VSOP58438, a low power preamplifier circuit for IR control centred at 38 kHz, useful to acquire IR signals from a high performance IR photodiode with a viewing angle of 110°.

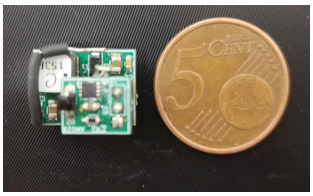

Figure 4.14: Wireless optogenetics circuit composed of two stage. The IR photodiode and the preamplifier circuit above and the microcontroller and harmonic oscillator circuit to drive the boost converter below. Here in comparison with 5 Euro Cents

The entire system dimensions are 15 x 11 mm and the weight is 1.75 g, instead the battery weight is 1.8 g.

To obtain a compact system, a relative protection from damage and mostly to avoid animal movements that could get stuck them inside the home-cage, I have planned also the realization of a plastic box (PLA). This plastic box allows me also to fix in place the battery.

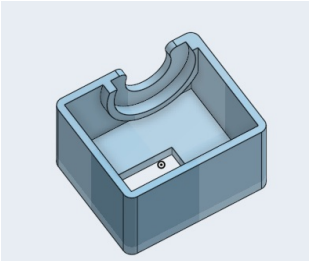

Figure 4.15: 3D drawing of the PLA box to protect the circuit.

4.3.1 IR protocol

The aim of this device is to allow a complete control of a wireless optogenetics experiment in social behavior paradigm. A low energy and power consumption device can not implement a Wi-Fi or Bluetooth module because of their high current consumption, while an IR wireless remote controller is the best choice.

Another advantage of using IR protocol is that we don't have radiofrequencies emitted inside the home-cage allowing, for example, future implementation of RFID identification.

With IR it is not needed any kind of antenna, only an IR photodiode to collect signals from an external control system.

However, the main problem of this technique is that between the emitter and the receiver there can not be any obstacle because, like visible light, infrared beams are blocked by physical constraints. So, the communication between the emitter and photodiode could not to be continuous.

Different IR protocols are used for TV remote controller, such as NEC, RC-5, X-SAT etc. but this protocols are too complex for this purpose in which I don't need to transfer a lot of information to the microcontroller.

So, I created a simple IR protocol in which the generated code is composed by only a byte composed of two hexadecimal digits; a first symbol to represent the interested animal (1 to 6) and a second symbol to represent the stimulation pattern (1 to 16) (Fig.4.16).

This code is then generated by a remote control circuit to drive an IR emitter. The IR photodiode on the wireless optogenetics circuit implanted

on each animal inside an home-cage receives the message, it decodes it and the selected stimulation pattern starts on the wanted animal.

IR Code	Frequency	Time Duration
A1	10 Hz	1 ms
A2	10 Hz	5 ms
A3	10 Hz	10 ms
A4	10 Hz	20 ms
A5	20 Hz	1 ms
A6	20 Hz	5 ms
A7	20 Hz	10 ms
A8	20 Hz	20 ms
A9	0.1 Hz	5 ms
A0	\	1 sec

Figure 4.16: IR protocols and corresponding optogenetics stimulation pattern.

These IR codes and stimulation patterns were used on the first *in vitro* tests performed in electrophysiology lab.

4.3.2 Infrared thermography

As mentioned previously in Section 4.2, the heat induction on the brain tissues could be a big problem. Thus, I tested the wireless optogenetics device using an infrared thermography camera (FLIR Systems) in order to detect infrared energy emitted from the tip of the optical system and directly from the electronic circuit (Fig.4.18).

To perform this test I injected to the high efficiency LED the maximum power that is possible to generate from the circuit using a laboratory power supply.

So, for this test I used these parameters:

- LED current = 30 mA;
- Voltage = 5 V;
- Optical power at the LED $\sim$ 5 mW;
- Optical power at the optical fiber tip $\sim$ 1.25 mW;
- Wavelenght = 475 nm;
- Fiber core diameter = 400 μm;
- LED radiant efficiency $\sim$ 12%;
- Total optical configuration efficiency $\sim$ 25%;

The optical prototype tested was then used for the first *in vitro* test (Fig.4.17).

From the results of the infrared thermography test it is possible to note how the temperature at the LED surface, at these operational conditions,

Figure 4.17: Image of the prototype for the optical system.

increased until 42.2 °C. On the fiber optic tip, after the positioning of the optical system, temperature decreased at 31.4 °C due to the thermal energy dissipation. Thus, confirming the proper operating conditions for the whole system.

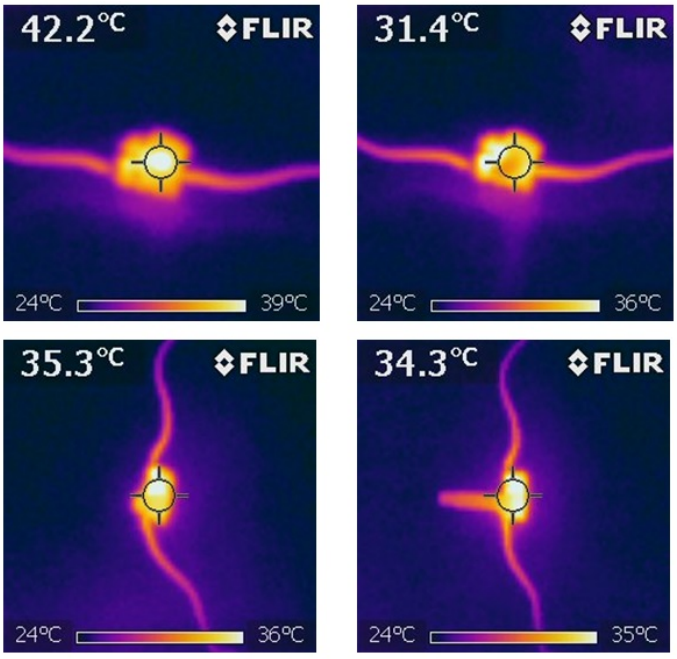

Figure 4.18: Infrared thermography. On the left the thermal response of the naked LED. On the right after the optical system implementation.

4.4 Electrophysiological results

Electrophysiology allows us to know in real time the electrical response of a neuron in terms of action potential activity. Channelrhodopsin-2 when photostimulated enables ion transit through the membrane ($H^+/Na^+/Ca^{2+}/K^+$).

These ions move from one side of the membrane to the other under the influence of an electrochemical gradient, triggering the generation of an electrical spike, called action potential, that is transmitted by the axon through a rapid changing in polarity across the cell membrane. The impulse travels down the axon in one direction only, to the axon terminal. At the end of each axonal branch is the presynaptic terminal, which contains vesicles filled with neurotransmitter. When an action potential reaches the terminal, the vesicular contents are released into the synaptic cleft allowing chemical communication with the postsynaptic cell.

Action potentials generated are modulated by the neuron on the basis of its physical characteristics, in fact its specific firing rate could be used as a marker and to understand behavioral response to drugs.

4.4.1 Patch clamp technique

The patch-clamp technique (Fig.4.19) is an electrophysiological method that allows the recording of whole-cell or single-channel currents flowing across biological membranes through ion channels. Using patch clamp we have the possibility to control and manipulate the voltage (voltage clamp) or the current (current clamp) of membrane patches or whole cells such as neurons. The basic approach to measuring small ionic currents in the picoampere range, as the transduction currents in neurons requires, a low-noise-recording technique combined with a precise mechanical positioning of the patch-clamp microelectrode are essential.

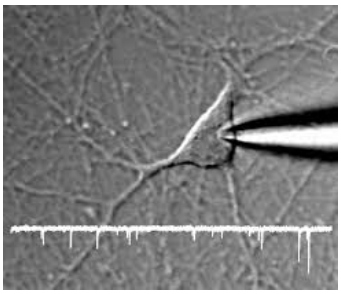

Figure 4.19: Patch clamp technique.

The electrical connection between microelectrode and preamplifier head-stage is kept as small as possible keeping the noise at a low level. Patch-clamp experiments require a precise and drift-free control of the movement

of the microelectrode. Therefore, the head stage is attached to the top of a three-dimensional micrometer screw-driven translation stage with a spatial resolution of about 1 μm in each direction. For vertical fine positioning of the patch pipette, the same piezo-electric device as that used for the specimen chamber was implemented into this translation stage. Thus, the vertical movement of the patch pipette and the investigated specimen are synchronized. A Faraday cage made of a metal grate shielding the microelectrode from electrical noise surrounds the whole setup. In voltage-clamp experiments the voltage across the membrane is measured and regulated with respect to a bath electrode. In these *in vitro* tests it was used the whole-cell recording technique, in which multiple channels current is recorded simultaneously. In this technique the electrode is left in place on the neuron and a suction is applied to rupture the membrane patch, thus providing access from the interior of the pipette to the intracellular space of the cell. The wireless optogenetics system was then positioned over the specimen chamber in which a 200 μm coronal rat brain slice was placed, the fiber optic tip was set up at a distance of $\sim$ 500 μm from the recorded neuron in the BLA.

4.4.2 Current clamp results

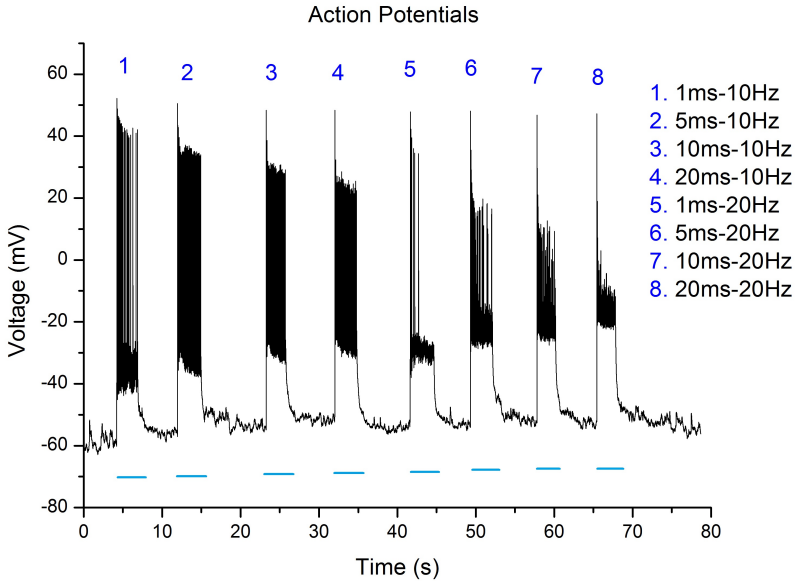

Figure 4.20: Current clamp results for the 10 Hz and 20 Hz stimulation patterns.

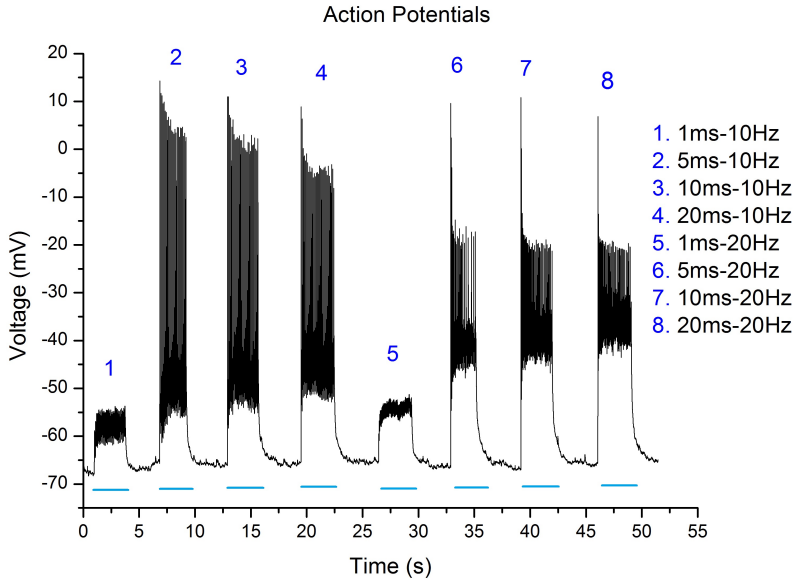

Figure 4.21: Current clamp results for the 10 Hz and 20 Hz stimulation patterns.

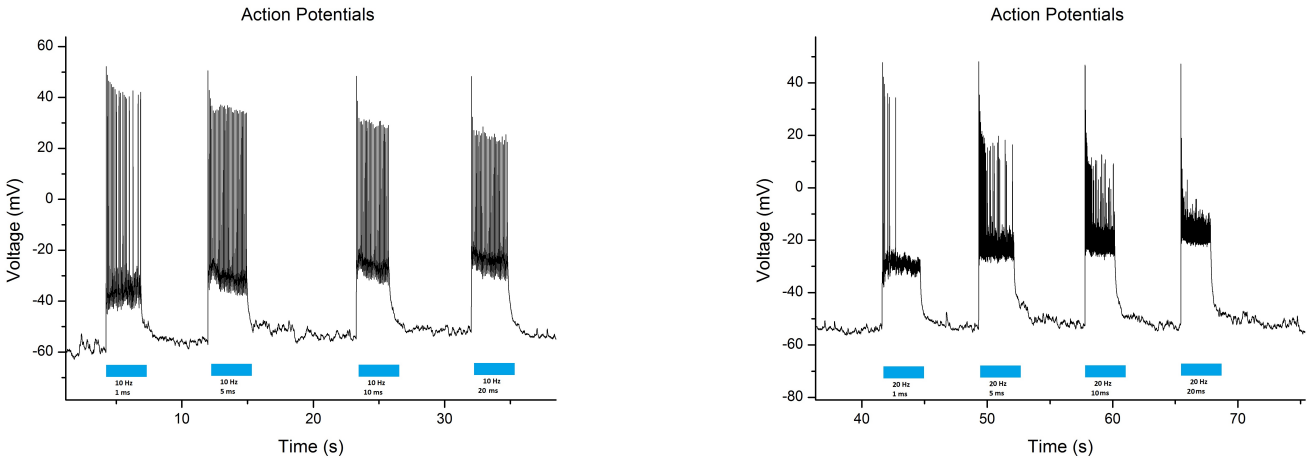

(a) **(b)**

Figure 4.22: Action potentials generated. **a)**10Hz stimulation for different high impulse time duration (1ms - 5ms - 10ms - 20ms). **b)**20Hz stimulation for different high impulse time duration (1ms - 5ms - 10ms - 20ms).

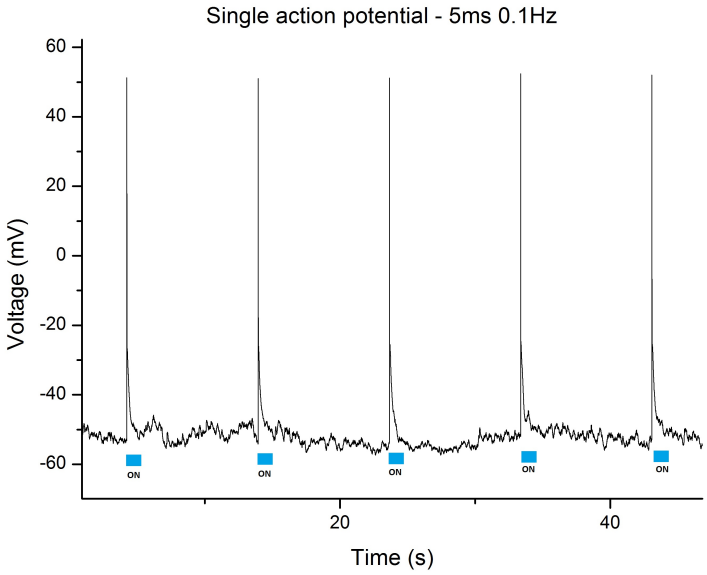

Figure 4.23: Single action potential generated by a stimulation pattern of 0.1 Hz and an high impulse of 5 ms.

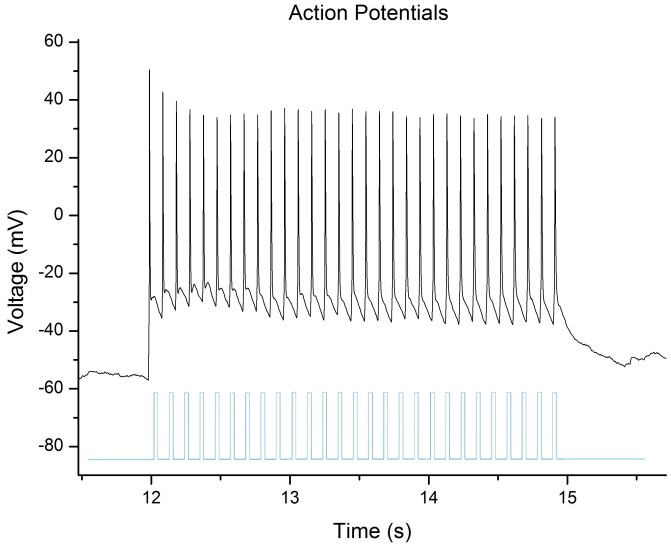

Figure 4.24: Action potentials generated by a 10 Hz frequency and 10 ms high impulse pattern.

These data were collected from BLA neurons of a 200 μm coronal rat brain slices.

Rats were injected with 0.5 μL viral vector *AAV-CaMKIIa-hChR2-mCherry* few weeks before the tests. Fluorescent protein *mCherry* were used in fluorescence microscopy to confirm the successful transfection of the virus. Fig.4.21 shows that for an high impulse time duration of 1 ms this neuron could not reach the threshold potential necessary to regulate and propagate signaling. This is probably due to a low optical power density on that region for a such short light pulse. It is possible to note also from electrophysiological data, especially from Fig.4.22-b, that a 20 Hz stimulation frequency is too high for that kind of neuron. This could be interpretated as a typical characteristic of these neurons.

4.4.3 Voltage clamp results

Contrary to the current clamp measurements, in voltage clamp the reference membrane potential is maintained at a specific voltage through a negative feedback and the current variation inside the cell membrane due to the opening of ion channels is measured.

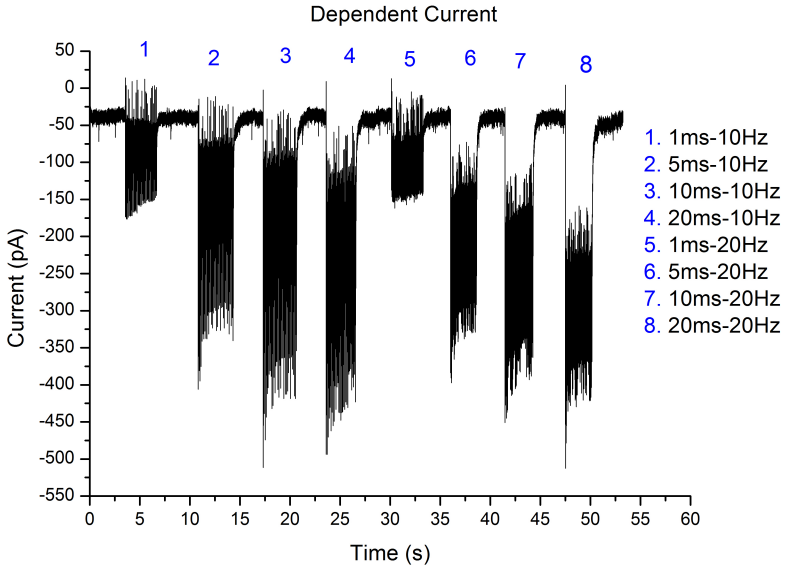

Figure 4.25: Voltage clamp result for the 10 Hz and 20 Hz stimulation patterns.

From previous data on current clamp and data in Fig.4.25 we can see that the best response in generating ion current is for frequency of 10 Hz and a high impulse of 10 ms.

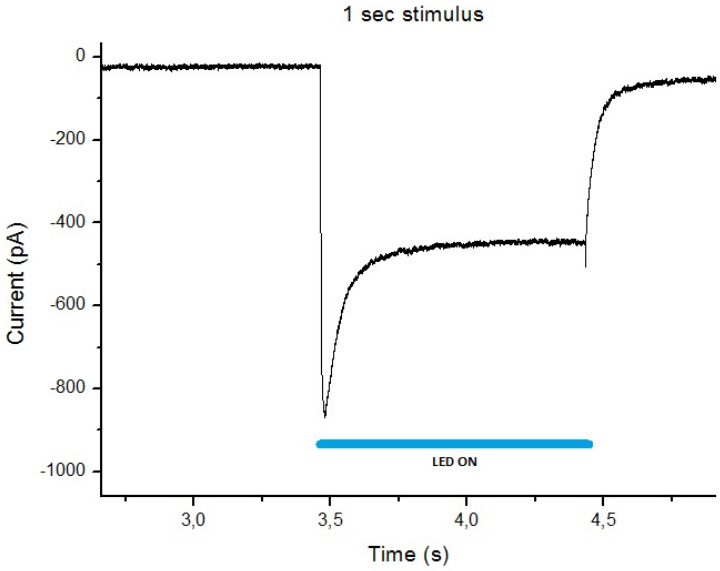

Figure 4.26: Ion current generated by a 1 second continuous light stimulus.

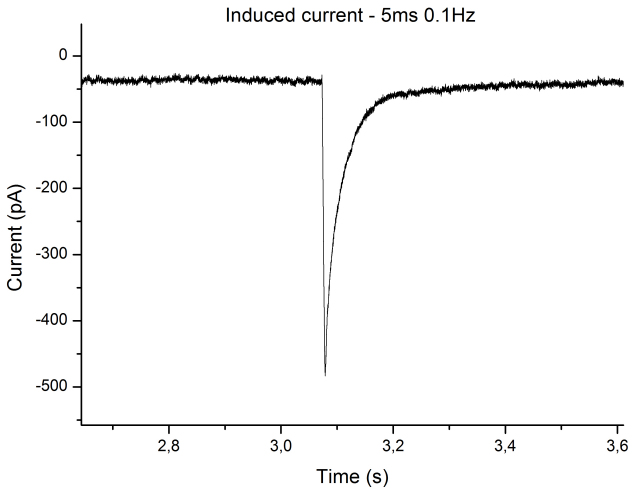

Figure 4.27: Ion current generated by a short single pulse of 5 ms light stimulus.

These preliminary data demonstrate the validity and effectiveness of this wireless optogenetics device to reach the activation threshold of the Channelrhodopsin-2. *In vivo* experiments will be performed in the future.

Chapter 5

Conclusions

The aim of the work of these three years has been fully achieved.

In conclusion, the collaboration with AM Microsystems turned out to be productive not only with the development of the liquid level sensor and its patent application, but also in other projects started from this experience.

The company is interested on the production and marketing of the liquid level device under their Chora Project and with the collaboration of the Italian Institute of Technology for what concerns other electronic devices aimed at animal experimentation.

Such as the feeder presented at the 'CRACK IT Challange' organized by the NC3R in UK with the MRC Harwell Institute as a sponsor.

Then, results obtained for Tecniplast were useful to have a complete validation analysis on their DVC®system. Furthermore, all tests performed are ready to be published in a technical publication. In the next future, Tecniplast is going to use these validation tests in their advertising for product launch.

The wireless optogenetics device is currently suitable for a patent application in collaboration with AM Microsystems. Furthermore it is available for next *in vivo* tests in our Pharmacology lab and other collaboration with research centers in order to perform social behavior experiments.

Bibliography

[1] Nuffield Council on Bioethics. The Ethics of Research Involving Animals - London: Nuffield Council on Bioethics; 2005. pp. 1 - 376

[2] Olsson IAS, Hansen AK, Sandoe P. *Animal welfare and the refinement of neuroscience research methods A case study of Huntingtons disease models.* Lab Anim. 2008;42:277283.

[3] Schuppli CA, Fraser D, McDonald M.*Expanding the Three Rs to meet new challenges in humane animal experimentation.* ATLA. 2004;32:525532.

[4] Conlee KM, Boysen ST. *Chimpanzees in research: Past, present and future.* In: Salem DJ, Rowan AN, editors. The State of the Animals III: 2005. Washington, DC: Humane Soc Pr; 2005. pp. 119133.

[5] de Boo MJ, Rennie AE, Buchanan-Smith HM, Hendricksen CFM. *The interplay between replacement, reduction and refinement: considerations where the Three Rs interact.* Anim Welfare. 2005;14:327332

[6] Griffin G, Gauthier C. *Incorporation of the principles of the Three Rs in wildlife research.* ATLA. 2004;32

[7] Everitt, J.I., Foster, P.M.D., 2004. *Laboratory animal science issues in the design and conduct of studies with endocrine-active compounds.* ILAR J. 45, 417425.

[8] Castelhano Carlos and Baumans, 2009. *The impact of light, noise, cage cleaning and in-house transport on welfare and stress of laboratory rats* Lab Anim

[9] E.Balzani, M.Falappa, F.Balci and V.Tucci, 2018. *An approach to monitoring home-cage behavior in mice that facilitates data sharing* Nature Protocol.

[10] Cook, Diane; Das, Sajal (2005). *Smart Environments: Technology, Protocols and Applications.* Wiley-Interscience.

[11] Lee Moir et al. *Disruption of the homeodomain transcription factor orthopedia homeobox (Otp) is associated with obesity and anxiety.* Molecular Metabolism, Volume 6, Issue 11, November 2017

[12] Jian Z. Chen, Anton A. Darhuber, Sandra M. Troian and Sigurd Wagner. *Capacitive sensing of droplets for microfluidic devices based on thermocapillary actuation.* Lab Chip [serial online] 2004; 4: 473480.

[13] David Wang. *Capacitive Sensing: Out-of-Phase Liquid Level Technique.* Application Report. Texas Instruments. http://www.ti.com/lit/an/snoa925/snoa925.pdf

[14] *http://web.jhu.edu/animalcare/procedures/mouse.html* - *http://web.jhu.edu/animalcare/procedures/rat.html*

[15] A.W.Johnson, A. Sherwood, D.R. Smith, M. Wosiski-Kuhn, M. Gallagher, and P.C. Holland. *An analysis of licking microstructure in three strains of mice.* Appetite. 2010 Apr; 54(2): 320330.

[16] J. D. Boughter, J.P. Baird, J. Bryant, S. J. St. John, D. Heck. *C57BL/6J and DBA/2J mice vary in lick rate and ingestive microstructure* Genes, Brain and Behavior (2007) 6: 619627.

[17] F.H. Crick *Thinking about the brain* Sci. Am., 241 (1979), pp. 219-232

[18] A. Matsuno-Yagi, Y. Mukohata *Two possible roles of bacteriorhodopsin; a comparative study of strains of Halobacterium halobium differing in pigmentation* Biochem. Biophys. Res. Commun., 78 (1977), pp. 237-243

[19] G. Nagel, D. Ollig, M. Fuhrmann, S. Kateriya, A.M. Musti, E. Bamberg, P. Hegemann *Channelrhodopsin-1: a light-gated proton channel in green algae* Science, 296 (2002), pp. 2395-2398

[20] E.S. Boyden, F. Zhang, E. Bamberg, G. Nagel, K. Deisseroth *Millisecond-timescale, genetically targeted optical control of neural activity* Nat. Neurosci., 8 (2005), pp. 1263-1268

[21] Joseph M. Stujenske, Timothy Spellman,Joshua A. Gordon *Modeling the Spatiotemporal Dynamics of Light and Heat Propagation for In Vivo Optogenetics* Cell Reports Volume 12, Issue 3, 21 July 2015, pp 525-534

[22] Gabriel Gagnon-Turcotte ; Yoan LeChasseur ; Cyril Bories ; Youns Messaddeq ; Yves De Koninck and Benoit Gosselin *A Wireless Headstage for Combined Optogenetics and Multichannel Electrophysiological Recording* IEEE TRANSACTIONS ON BIOMEDICAL CIRCUITS AND SYSTEMS Volume 11, Issue 1, Feb. 2017, pp 1 - 14

[23] Li Yang and Stanley J. Miklavcic *Revised KubelkaMunk theory. III. A general theory of light propagation in scattering and absorptive media* Journal of the Optical Society of America A Vol. 22, Issue 9, pp. 1866-1873 (2005)

[24] Yuming Liu, Steven L. Jacques, Mehdi Azimipour, Jeremy D. Rogers, Ramin Pashaie, and Kevin W. Eliceiri *OptogenSIM: a 3D Monte Carlo simulation platform for light delivery design in optogenetics* Biomedical Optics Express Vol. 6, Issue 12, pp. 4859-4870 (2015)

[25] Thomas Knopfel, Edward S. Boyden *Optogenetics: Tools for Controlling and Monitoring Neuronal Activity (Progress in Brain Research)* Volume 196, Pag.224, January 2012

[26] Frederic Bevilacqua, Dominique Piguet, Pierre Marquet, Jeffrey D. Gross, Bruce J. Tromberg, and Christian Depeursinge *In vivo local determination of tissue optical properties: applications to human brain* Applied Optics. Vol. 38, No. 22, pp. 4939-4950, 1 August 1999

[27] APTD1608LVBC/D Blue (InGaN) KINGBRIGHT Datasheet

[28] http://donklipstein.com/photopic.html

[29] ATMEL ATtiny43u Datasheet

[30] Kyung Nim Noh, Sung Il Park, Raza Qazi, Zhanan Zou, Aaron D. Mickle, Jose G. Grajales-Reyes, Kyung-In Jang, Robert W. Gereau IV, Jianliang Xiao, John A. Rogers and Jae-Woong Jeong *Miniaturized, Battery-Free Optofluidic Systems with Potential for Wireless Pharmacology and Optogenetics* Small 2018, 14, 1702479